Marine and Petroleum Geology 137 (2022) 105499

Contents lists available at ScienceDirect

Marine and Petroleum Geology

journal homepage: www.elsevier.com/locate/marpetgeo

Reservoir solid bitumen-source rock correlation using the trace and rare earth elements–implications for identifying the natural gas source of the Ediacaran-Lower Cambrian reservoirs, central Sichuan Basin

Lianqiang Zhu [a,b], Guangdi Liu [a,b,**], Zezhang Song [a,b,*], Wenzhi Zhao [a,b], Qiang Li [a,b], Xingwang Tian [c], Yunlong Wang [c], Dailin Yang [c]

[a] State Key Laboratory of Petroleum Resources and Prospecting, China University of Petroleum, Beijing 102249, PR China
[b] College of Geosciences, China University of Petroleum, Beijing 102249, PR China
[c] Southwest Oil and Gas Field Company PetroChina, Chengdu 610041, PR China

ARTICLE INFO

Keywords:
Reservoir solid bitumen-source rock correlation
Trace elements
Rare earth elements (REE)
The Ediacaran-lower Cambrian
Central Sichuan

ABSTRACT

The hydrocarbon-source correlation in highly-mature and over-mature stages is a challenging task in natural gas exploration. The Ediacaran-Lower Cambrian natural gas in the central Sichuan Basin is typical oil-cracking gas. With a burial depth of more than 4650 m, the gas is now in the highly-mature to the over-mature stage (equivalent Ro>1.8%) with apparent alteration by thermochemical sulfate reduction (TSR), leading to difficulties for gas-source correlation. Conventional hydrocarbon-source correlation mainly relies on organic geochemical methods, taking media such as biomarkers and carbon isotope for correlation. However, in the highly-mature and over-mature stages, the characteristics of conventional biomarkers tend to be homogenised. Furthermore, the gas components and carbon isotope of natural gas are frequently altered by TSR in the deep burial stage. Thus, conventional organic geochemical methods are significantly restricted. This paper explored the source of highly-mature natural gas from the DY and LWM Formations in the central Sichuan Basin by studying the inorganic geochemical information (trace elements and rare earth elements) of the reservoir bitumen and potential source rocks. The results show that the depositional environment of the potential source rocks (the QZS and the D-3 source rocks) in the central Sichuan Basin were different. The redox-sensitive parameters (V/(V + Ni), Mo/Ni, δCe and Ce/Y) and the provenance-sensitive parameters (La/Co and La/Sc) of the source rocks have apparent differences, which can be used as the basis for gas-source correlation. The correlation results show that the LWM gas was derived from the QZS source rock, while the D-2 and D-4 gases were mainly derived from the QZS source rock, with a partial contribution of the D-3 source rock. During geologic evolution, the crude oil generated from the two sets of source rocks were thoroughly mixed in the paleo-oil reservoir of the D-4 Member. As a result, the characteristics of the D-3 source rock were obscured by the QZS. In contrast, the solid bitumen in the D-2 paleo-oil-reservoir recorded the contribution of the D-3 source rock. However, this contribution was limited within the range of 50 m adjacent to the D-3 Member by a more significant oil generation from the QZS source rock located in Deyang-Anyue Rift Trough. This study clarified the gas source differences between the D-2 Member, D-4 Member and LWM Formation, providing a new insight for in-depth study on the gas accumulation of the Ediacaran-Lower Cambrian in the central Sichuan Basin.

1. Introduction

The organic hydrocarbon generation theory believes that oil and gas are mainly of organic origin. Therefore, the organic geochemical methods have been widely utilised in the oil/gas and source correlation (Zhu et al., 2003, 2007; Dai et al., 2005; Ma, 2008), and have made remarkable achievements for identifying the source of the low-medium mature hydrocarbon (Zhang et al., 2002; Mei et al., 2008; Cheng et al., 2021; Hou et al., 2021). However, when hydrocarbon locates in the highly-mature to the over-mature stages, most biomarkers (isoprenoid

* Corresponding author. State Key Laboratory of Petroleum Resources and Prospecting, China University of Petroleum, Beijing 102249, PR China.
** Corresponding author. State Key Laboratory of Petroleum Resources and Prospecting, China University of Petroleum, Beijing 102249, PR China.
E-mail addresses: lgd@cup.edu.cn (G. Liu), songzz@cup.edu.cn (Z. Song).

https://doi.org/10.1016/j.marpetgeo.2021.105499
Received 28 September 2021; Received in revised form 22 November 2021; Accepted 21 December 2021
Available online 23 December 2021

alkanes, steranes, terpenes, etc.) can no longer indicate the parent source (Liang and Chen, 2005). In addition, crude oil has cracked into dry gas in the highly-mature to over-mature stages. As a result, only a few organic geochemical parameters (carbon isotopes, light hydrocarbons, etc.) can be used for gas-source correlation.

Except for natural gas, another product is formed by crude oil cracking in highly-mature to over-mature stages—solid bitumen. Theoretically speaking, natural gas and solid bitumen have the same source in unmixed gas and bitumen. Compared with natural gas, solid bitumen usually carries richer source information. Therefore, solid bitumen-source correlation can indicate the gas source in highly-mature to over-mature areas (Holman et al., 2014; Connan et al., 1995; Manzano et al., 1997; Mankiewicz et al., 2009; Cai et al., 2013).

However, it is challenging to correlate the gas and source in highly-mature to over-mature areas (Tissot and Welte, 1984; Hunt, 1996; Huang, 1996). In the deeply buried stage, TSR alteration occurs in many gas reservoirs (Zhu et al., 2005, 2006; Dai et al., 2005). TSR alteration always prioritises the consumption of heavier natural gas (C_2H_6, C_3H_8) in gas reservoirs and is accompanied by obvious carbon isotope fractionation, leading to significant changes in the components and isotopes of natural gas. In addition, applying highly-mature and over-mature reservoir solid bitumen for hydrocarbon and source correlation faces the same problem—conventional biomarkers extracted from the solid bitumen tend to be similar, carbon isotopes are changed under TSR alteration and can hardly reflect the actual information of the source. As such, in highly-mature to over-mature areas, conventional organic geochemical parameters (biomarkers, carbon isotope, etc.) for gas and source correlation have been modified to varying degrees, resulting in the limitation of organic geochemical methods in gas-source and gas-bitumen-source correlations (Liang and Chen, 2005; Wang and Han, 2011; Shi et al., 2017).

In 2013, the Anyue Ediacaran-Lower Cambrian giant gas field was established in the central Sichuan Paleo-uplift, Sichuan Basin. The main gas producing layers are the Dengying (DY) and the Longwangmiao (LWM) Formations (Wei et al., 2014; Zou et al., 2015). Natural gas from the DY and LWM Formations in the central Sichuan Basin is oil-cracking gas formed in highly-mature to over-mature stages. The potential source rocks include the Ediacaran Doushantuo (DST) Formation (mudstone), the third Member of Dengying Formation (mudstone, D-3 Member) and the Cambrian Qiongzhusi (QZS) Formation (shale) (Wei et al., 2015b, 2017; Wu et al., 2016; Shi, 2017; Shi et al., 2017). Gas-source and gas-bitumen-source correlation methods have been widely used to study natural gas sources for the DY and LWM Formations. To date, the natural gas source of the LWM Formation has reached a unified understanding—the QZS source rock. However, there are still controversies on the gas source of the DY Formation.

Though various organic geochemical methods have been applied and confirmed the contribution of QZS source rock to the natural gas of the DY Formation, there are different opinions on the contribution of the D-3 source rock (Zheng et al., 2014; Wei et al., 2015a; Yang et al., 2016; Xie et al., 2021; Wu et al., 2016). The equivalent *Ro* (Vitrinite reflectance) values of the QZS and D-3 source rocks ranges from 1.8% to 3.2%, indicating a highly-mature to over-mature stages. Reservoir bitumen obtained from the LWM and DY Formations are also in highly-mature to over-mature stages (equivalent $Ro>1.8\%$), and the gas reservoir is mainly composed of CH_4 (Zhu et al., 2005; Wei et al., 2015a, 2017). At such a stage, conventional biomarkers (terpanes, steranes, etc.) in source rocks and reservoir bitumen may become homogeneous, showing strong similarities (Xu et al., 2012). In addition, as the natural gas of the DY Formation had experienced apparent TSR alteration, the H_2S concentration in DY natural gas is relatively high, ranging from 8.83 to 35.13 g/m^3 (Zhu et al., 2021). The carbon isotope of ethane is even heavier than the potential source rock, while the carbon isotope of reservoir bitumen is lighter (Wei et al., 2015a; Zhang, 2019; Zhang et al., 2019; Shuai et al., 2019; Song et al., 2020). Under the combined effect of these factors, the geochemical characteristics of carbon isotope and biomarkers in natural gas and reservoir bitumen may have lost the capability to indicate the parent source rock, leading to the diversified results of gas-source correlation led by organic geochemical methods.

In fact, in addition to the widespread organic components in crude oil and reservoir bitumen, there are also some inorganic components, including trace elements and rare earth elements (REE) (Gao et al., 2017; Shi, 2017; Roth et al., 2017). These inorganic components have a certain degree of stability during crude oil migration. Although the alteration (such as thermal alteration, biodegradation, etc.) and migration may change the concentration of trace elements and REE in crude oil and solid bitumen, the ratio of certain elements does not change (Ramirez-Caro, 2013; Gao et al., 2017; Shi et al., 2017; Roth et al., 2017). Thus, the ratio of certain elements is a potential index for hydrocarbon and source correlation. At present, the inorganic geochemical method has been applied to hydrocarbon source correlation in the low-medium mature areas, and significant achievements have been obtained in basins such as the Junggar and the Anadarko basins (Cao et al., 2007, 2009, 2012; Ramirez-Caro, 2013; Roth et al., 2017). In recent years, inorganic methods have also been applied to studying the hydrocarbon and source correlation in highly-mature areas such as the Sichuan Basin and have made some breakthroughs (Li et al., 2014; Shi, 2017; Gao et al., 2017). These successful examples provide a brand-new start for studying natural gas sources in highly-mature to over-mature areas based on inorganic geochemistry.

Given the enormous challenges conventional organic geochemical methods faced for hydrocarbon and source correlation in the central Sichuan Basin, this study applied inorganic geochemical methods to study the reservoir bitumen source of the DY and LWM Formations. In the study, the QZS and D-3 source rocks were better distinguished by trace elements and REE. Based on the correlation of the trace elements and REE in the reservoir bitumen and potential source rocks, the natural gas sources of the LWM and DY Formations were discussed. The successful application of inorganic geochemical methods in gas and source correlation in the complex superimposed basin in Sichuan provides a new example for studying natural gas sources in highly-mature to over-mature areas.

2. Geological setting

The Central Sichuan Paleo-uplift formed during the Caledonian tectonic movement, and its axis is located on the Yaan-Ziyang-Yuechi line. The structural features of the various layers before the Permian in the Paleo-uplift area generally appear like a vast nose-like uplift that sinks in the NEE direction (Xu et al., 2012; Li et al., 2014; Mei et al., 2014). The study area is located in the central Sichuan Basin, including the Uplift Area and North Slope of the Paleo-uplift (Fig. 1). From the perspective of the current structure, the Uplift Area is mainly composed of Moxi and Gaoshiti structures, while the North Slope mainly refers to the monoclinic structural belt in the northern area of the Moxi structure, with the Deyang-Anyue Rift Trough on the west side and Jiulongshan on the north side (Fig. 1) (Ma et al., 2020).

Both the DY Formation and the LWM Formation are carbonate strata. From bottom to top, the Ediacaran DY Formation can be divided into four Members, namely D-1, D-2, D-3 and D-4 Members. Dissolved fractures and caves are developed in the D-2 and D-4 Members, while intergranular pores and inter-crystalline pores are developed in the LWM Formation, together constituting the main reservoir space of the Anyue large gas field (Fig. 1) (Wei et al., 2015b; Zou et al., 2015). The concentration of CH_4 of the DY reservoir is usually greater than 85%, the concentration of C_2H_6 is less than 0.3%, while the concentration of C_3H_6 is trace. The natural gas drying index is greater than 0.996, which indicates the highly mature natural gas (Wei et al., 2014; Du et al., 2015; Zou et al., 2015). Three sets of source rocks, including DST Formation, D-3 member and QZS Formation, have organic carbon concentration (TOC) of 2.91%, 0.87% and 1.97%, and are widely distributed in the study area, which is high-quality potential source rocks. The equivalent

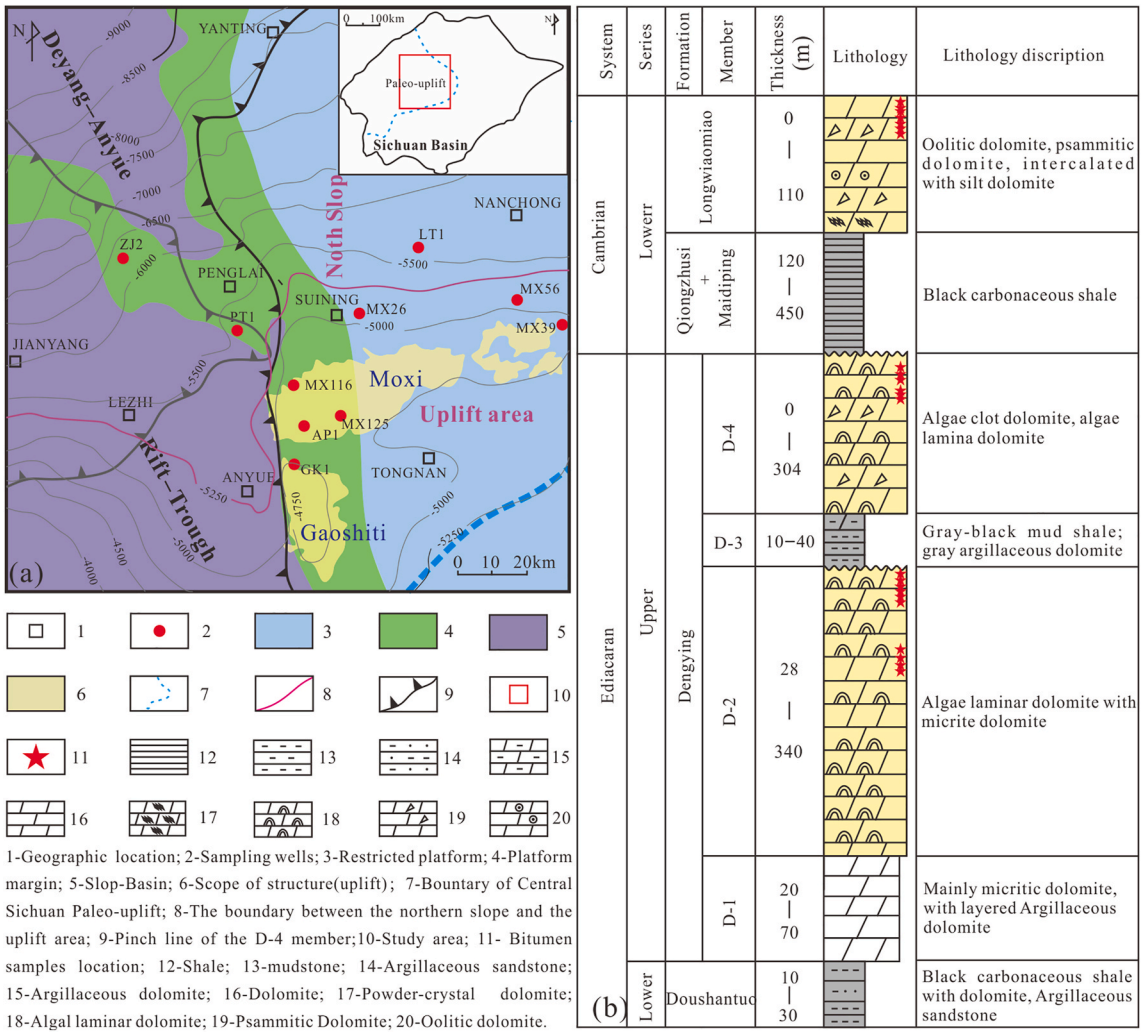

Fig. 1. Geological overview of central Sichuan Basin. (a) The location of the study area (modified by Zhao et al., 2020). The base map is the depositional facies of the DY Formation. (b) Stratigraphic column.

Ro of the source rocks exceeds 1.8% (Ro>1.8%), indicating that the potential source rocks are all in the highly-mature to over-mature stages (Wei et al., 2015b, 2017) (Fig. 1).

3. Samples and methods

3.1. Coring and sampling

The drilling core observation results showed a large amount of solid bitumen filled in the caves of the DY and LWM Formations (Fig. 2), which laid a good material foundation for the study on gas-bitumen-source correlation. Based on many drilling core observations, QZS and D-3 source rock were systematically sampled, and bitumen from the D-4, D-2 and LWM reservoirs. 13 source rock samples, 24 dolomite samples containing bitumen were finally sampled (Fig. 2). The samples cover seven wells (MX39, MX116, MX125, MX26, MX56, GK1, AP1) in the Moxi-Gaoshiti area and three wells (PT1, ZJ2, LT1) in the north slope of the central Sichuan paleo-uplift. Detailed sample information was exhibited in Table 1.

3.2. Sample preparation

To obtain solid bitumen samples, we broke the solid bitumen-containing dolomite block into small pieces of 3 mm–5 mm. Then, the solid bitumen particles separated from the dolomite were selected with wooden tweezers. Using a wooden tool, we removed the dolomite, quartz and other attached mineral fragments on the surface of the solid bitumen under the microscope. We put the obtained bitumen pieces into a small beaker containing deionised water, cleaned them in 50Hz ultrasonic waves for 1 h, and then ventilated and dried them in a drying oven at 80 °C for 5 h. Finally, we used an agate mortar to grind the solid bitumen to 200 meshes for geochemical analysis.

3.3. Experimental method

Trace elements and REE are analysed and tested in the Beijing Institute of Geology of Nuclear Industry, China, with a Thermo Scientific Element XR inductively coupled plasma mass spectrometer. During the experiment, 10 ng Rh was used as the online internal standard, and the repeated measurement of the laboratory rock standard sample was used to control the analysis accuracy. The analysis error of trace elements is less than 5%, and the analysis error of REE is less than 10%. To eliminate the odd-even effect of REE, we adopted the Post-Archean Australian Shale (PAAS) for REE normalisation.

4. Results

4.1. Trace elements

The concentration of trace elements of the QZS source rock has a

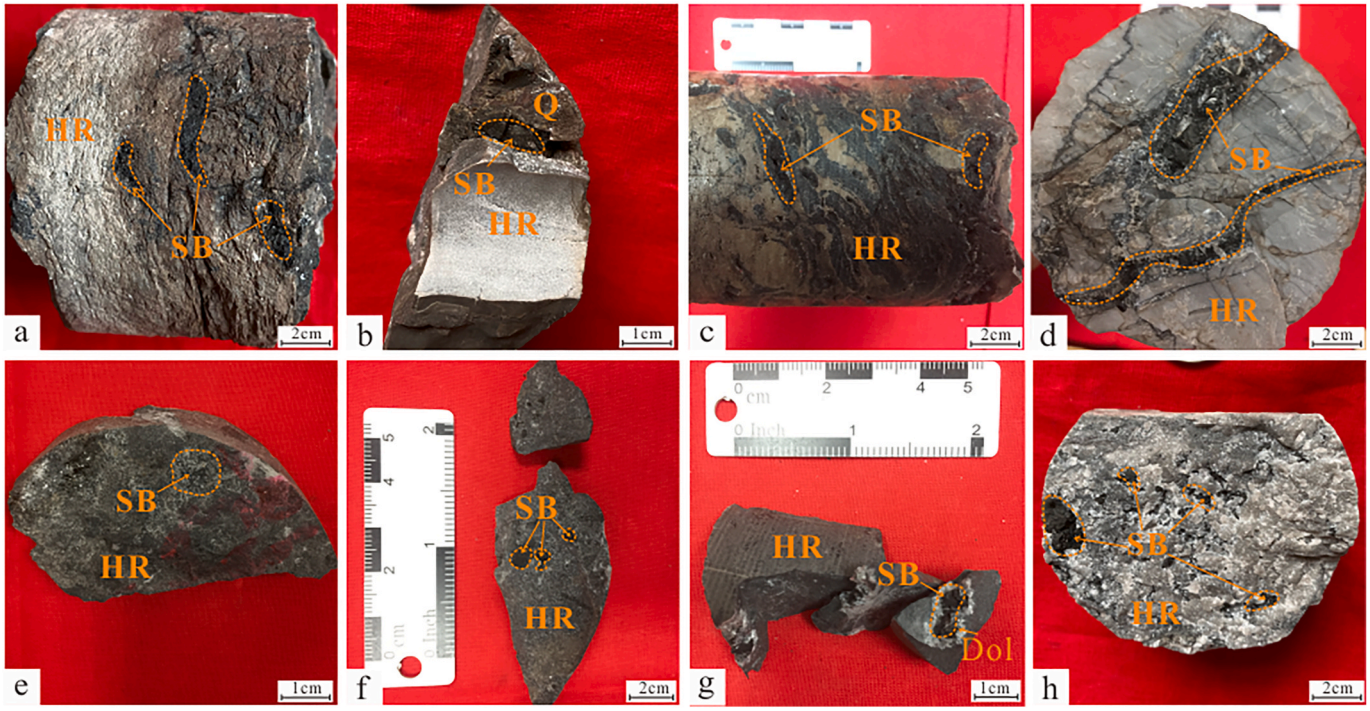

Fig. 2. The occurrence characteristics of solid bitumen in the DY and LWM Formations.
HR-host rock; SB-solid bitumen; Q-quartz; Dol-dolomite; (a) MX39, 5307.2 m, D-4 Member, caves in the dolomite are filled entirely with massive solid bitumen; (b) PT1, 5733.9 m, D-2 Member, caves in the dolomite are fully filled with bulk bitumen and megacryst quartz; (c) MX116, 5125.7m, D-4 Member, algae grid holes are filled with bulk bitumen, and the honeycomb pores inside the bitumen are developed; (d) MX125, 5334.7m, D-4 Member, there are two cracks in the core, with a width of 0.5 cm–2cm. A minor fine-medium crystalline dolomite is developed at the edge of the crack, which is then fully filled with massive solid bitumen; (e) MX26, 4913.5m, LWM Formation, inter-crystalline pores are developed and were filled with small pieces of bitumen; (f) MX56, 4963.6m, LWM Formation, caves were filled entirely with massive bitumen; (g) LT1, 5475.6m, LWM Formation, mesocrystalline dolomite grown at the edge of the caves, and the remaining caves were then half-filled with massive solid bitumen; (h) ZJ2, 6553.6m, D-2, caves and inter-crystalline pores were filled with massive bitumen.

mean value of 696.6 μg/g (ranging from 607.5 μg/g to 835.9 μg/g), while that of the D-3 source rock is significantly lower, only with a mean value of 318.2 μg/g (ranging from 88.7 μg/g to 525.6 μg/g). The concentrations of trace elements of the D-4 reservoir bitumen, D-2 reservoir bitumen and LWM reservoir bitumen are relatively close, with mean values of 558.4 μg/g (ranging from 355.9 μg/g to 702.7 μg/g), 521.7 μg/g (210.5 μg/g to 1365.8 μg/g) and 763.8 μg/g (230.1 μg/g to 2320.3 μg/g), respectively, showing significant similarity to the QZS source rock (Table 1). The distribution characteristics of trace elements of all source rock and reservoir bitumen samples show a certain similarity (Fig. 3). Compared with the Post-Archean Australian Shale (PAAS), the source rock and reservoir bitumen in the study area are enriched in V, Ni and Mo, are depleted in Rb and Cs (Fig. 3). There is a specific difference between the QZS and D-3 source rocks. Compared with adjacent elements, the Mo enrichment in the QZS source rock is significantly higher than the D-3 source rock. The D-2, D-4 and LWM reservoir bitumen show the high similarity in trace elements distribution pattern. Compared with adjacent elements, Rb and Cs elements are significantly depleted in these reservoirs, while Mo is significantly enriched, which is similar to the QZS source rock (Fig. 3).

4.2. Rare earth elements (REE)

4.2.1. REE concentration

The concentrations of REE of the D-3 and QZS source rocks are similar and significantly higher than that of the D-2, D-4 and LWM reservoir bitumen. The REE concentration of the QZS source rock has a mean value of 188.1 μg/g (ranging from 81.2 μg/g to 529.1 μg/g). Moreover, the REE concentration of the D-3 source rock is similar, with a mean value of 159.7 μg/g (ranging from 21.2 μg/g to 303.3 μg/g). The REE concentrations of the LWM Formation, D-4 Member, and D-2 reservoir bitumen are similar, with a mean value of 5.4 μg/g (0.8 μg/g~19.4 μg/g), 2.4 μg/g (0.3 μg/g~9.9 μg/g) and 2.8 μg/g (0.6 μg/g~6.9 μg/g), respectively, which are lower than that of the source rocks (Table 2).

4.2.2. Ce anomaly

When Bau and Dulski (1996) used the formula $\delta Ce = 2Ce_{SN}/(La_{SN} + Pr_{SN})$ to calculate the Ce anomaly in the Late Archean and Early Proterozoic iron Formation, they found that the La anomaly would affect the calculation results of the Ce anomaly, and then they proposed the method to distinguish the true and false Ce anomaly (Bau and Dulski, 1996). Fig. 4 is the identification chart, which can be divided into five areas: area I indicates no La and Ce anomaly, with $0.95 < \delta Pr < 1.05$ and $0.95 < \delta Ce < 1.05$; II indicates positive La anomaly and no Ce anomaly, with $0.95 < \delta Pr < 1.05$ and $\delta Ce < 0.95$; III indicates negative La anomaly and no Ce anomaly, with $0.95 < \delta Pr < 1.05$ and $\delta Ce > 1.05$; Ⅳ indicates normal positive Ce anomaly, with $\delta Pr < 0.95$ and $\delta Ce > 1.05$; Ⅴ indicates negative Ce anomaly, with $\delta Pr > 1.05$ and $\delta Ce < 0.95$.

The mean value of δCe in the QZS source rock is about 0.82 (ranging from 0.26 to 1.04), and the mean value of δPr is about 1.06 (ranging from 0.96 to 1.36). Most of the QZS Formation samples distribute in area I and II, indicating no Ce anomaly. One sample falls in the top of area Ⅴ is close to area I, showing a weak Ce anomaly. Different from most samples, two samples fall in area Ⅴ, indicating a negative Ce anomaly. The mean value of δCe in the D-3 source rock is about 0.43 (ranging from 0.30 to 0.51), while that of δPr is about 1.20 (ranging from 1.12 to 1.28). All the D-3 samples are distributed in area Ⅴ, indicating negative Ce anomalies. The QZS source rock mainly shows no Ce anomaly, while the source rock of the D-3 Member shows a negative Ce anomaly (Fig. 4).

The mean value of δCe of the D-4 reservoir bitumen is 0.92 (ranging from 0.67 to 1.19), and the mean value of the δPr is 0.93 (ranging from

Table 1
Trace element composition of source rock and solid bitumen, central Sichuan Basin.

Samples	Well	Formation	Depth	Object	Sc	V	Cr	Co	Ni	Cu	Zn	Ga	Rb	Sr	Mo	Cs
					μg/g											
ZJ2-1R	ZJ2	QZS	6327.9	Source	10.7	123.0	101.0	16.6	93.6	39.9	85.3	16.3	106.0	115.0	17.6	6.6
ZJ2-2R			5917.1	Rock	7.5	75.2	178.0	7.8	24.7	14.5	51.0	12.6	78.6	95.7	3.9	3.4
ZJ2-3R			5912.5		6.6	152.0	113.0	21.6	74.1	27.6	133.0	11.4	72.9	98.6	15.5	3.4
ZJ2-4R			5911.1		7.1	92.8	241.0	14.1	46.1	26.0	61.0	12.1	73.5	96.8	9.5	3.6
PT1-1R	PT1		5590.5		1.9	38.9	58.6	1.6	19.0	10.3	18.7	2.9	14.8	617.0	1.7	0.2
PT1-2R			5589.5		1.6	144.0	80.2	2.0	20.0	20.0	19.9	2.7	6.8	535.0	3.7	0.1
PT1-3R			5305.9		8.1	104.0	312.0	10.5	43.9	25.1	51.3	13.4	79.0	107.0	8.6	3.3
PT1-4R			5305.7		10.6	151.0	208.0	22.2	56.2	35.7	70.0	15.6	83.2	155.0	10.9	3.9
AP1-1R*	AP1		5030.0		7.4	142.0	71.0	13.5	64.0	33.0	37.0	14.7	106.0	82.0	32.0	4.9
AP12R*			5031.1		7.2	158.0	68.0	12.4	76.0	28.5	47.0	13.0	98.0	84.0	21.9	4.5
AP1-3R*			5033.2		11.3	127.0	78.0	13.3	70.0	31.0	46.0	16.3	119.0	82.0	17.3	6.0
AP1-4R*			5035.1		12.7	121.0	81.0	13.8	71.0	36.0	28.0	17.4	129.0	74.0	18.6	6.4
GK1-1R	GK1	D-3	5052.0		0.2	14.8	17.1	0.9	11.9	0.5	8.3	0.3	0.5	33.9	0.3	0.0
GK1-2R			5147.6		0.4	22.1	32.2	1.1	12.3	1.7	4.6	0.8	2.2	42.3	0.4	0.1
GK1-3R			5179.6		0.4	24.3	30.1	1.0	13.6	1.7	6.1	0.8	2.0	36.1	0.4	0.1
GK1-4R			5351.9		6.0	59.5	74.8	9.0	51.8	34.8	21.9	12.2	68.3	79.2	2.3	3.7
GK1-5R			5350.0		4.3	48.0	37.7	5.3	27.9	14.1	19.3	6.8	39.7	91.7	1.5	1.9
GK1-1R*			5351.9		9.7	73.0	63.0	9.0	57.0	28.9	22.6	13.0	77.0	117.0	2.5	4.1
GK1-2R*			5353.3		9.9	87.0	76.0	11.0	74.0	32.0	25.4	15.6	87.0	99.0	3.7	5.0
GK1-3R*			5356.2		10.5	80.0	76.0	11.9	56.0	34.0	25.5	16.6	104.0	100.0	2.6	5.5
GK1-4R*			5357.0		3.5	22.1	23.6	3.5	27.8	9.4	11.0	4.4	25.6	89.0	0.8	1.1
GK1-5R*			5357.6		7.2	59.0	49.0	8.8	42.0	26.9	19.7	10.3	64.0	96.0	2.2	3.1
MX39-1B	MX39	D-4	5307.2	Reservoir Bitumen	0.1	273.0	17.4	0.5	184.0	9.8	121.0	2.0	0.5	33.1	61.3	0.0
MX39-2B			5301.0		0.1	246.0	20.6	0.2	139.0	3.0	63.2	1.4	0.5	23.7	28.0	0.1
MX39-3B			5284.7		0.2	283.0	19.3	0.3	167.0	2.9	42.3	1.2	0.7	26.3	36.0	0.1
MX39-4B			5267.2		0.1	302.0	8.1	0.2	150.0	0.4	18.5	1.3	0.1	3.8	43.4	0.0
MX116-1B	MX116		5125.7		0.8	315.0	38.7	0.7	152.0	3.6	112.0	1.5	0.7	101.0	32.6	0.1
MX125-1B	MX125		5334.7		0.6	214.0	20.1	0.3	106.0	0.6	7.2	1.2	0.3	23.4	20.3	0.0
GK-1B*	GK1		5178.3		0.4	173.0	13.2	0.6	104.0	3.1	13.4	0.7	4.0	20.1	23.4	0.1
AP-1B*	AP1		5040.8		0.3	335.0	6.6	0.3	197.0	2.2	8.6	0.2	2.7	25.0	45.0	0.0
PT1-1B	PT1	D-2	5741.1		0.2	185.0	24.2	0.7	110.0	108.0	14.1	0.6	0.3	119.0	13.8	0.0
PT1-2B			5733.9		0.1	213.0	14.5	0.5	115.0	40.4	449.0	0.9	0.2	52.0	17.3	0.0
PT1-3B			5733.3		0.2	85.6	54.0	0.4	90.0	1.7	111.0	0.7	0.3	43.4	19.8	0.0
PT1-4B			5730.0		0.1	54.8	29.2	0.9	33.8	1131.0	/	61.7	0.5	48.8	4.9	0.1
ZJ2-1B	ZJ2		6553.6		0.1	64.2	4.7	0.1	98.1	0.7	17.7	2.5	0.3	18.1	3.9	0.1
ZJ2-2B			6551.5		0.7	69.3	8.4	0.3	103.0	2.5	122.0	2.4	0.3	53.4	3.1	0.1
ZJ2-3B			6550.7		0.1	110.0	9.2	0.5	101.0	2.9	32.0	2.7	0.8	294.0	7.6	0.3
ZJ2-4B			6547.2		0.2	88.1	5.9	0.2	106.0	0.6	12.1	2.4	0.7	19.1	6.8	0.1
ZJ2-5B			6546.5		0.1	99.3	5.1	0.3	114.0	1.0	9.4	2.6	0.9	39.6	16.3	0.2
ZJ2-6B			6546.3		0.1	132.0	6.5	0.1	111.0	0.5	4.4	2.9	0.4	28.3	10.9	0.3
LT1-1B	LT1	LWM	5471.8		0.5	400.0	27.1	0.3	127.0	0.5	5.7	4.5	0.7	1.7	12.0	0.0
LT1-2B			5475.6		0.9	204.0	29.8	0.6	70.8	1.0	5.4	3.8	0.8	333.0	4.3	0.0
MX26-1B	MX26		4913.5		0.5	124.0	20.3	0.1	28.8	30.6	3.4	3.1	0.3	17.1	1.8	0.0
MX26-2B			4910.3		0.5	128.0	31.7	0.7	34.4	16.4	20.1	2.4	1.0	84.4	4.8	0.2
MX26-3B			4968.6		1.24	165	305	2.42	45	21.2	132	4.21	3.72	1634	5.88	0.623
MX56-1B	MX56		4952.9		0.755	184	35.8	0.484	91.1	1.36	16.3	1.91	1.22	126	14.2	0.375

Note: QZS = Qiongzhusi Formation, D-3 = 3rd Member of the Dengying Formation, D-4 = 4th Member of the Dengying Formation, D-2 = 2nd Member of the Dengying Formation, LWM = Longwangmiao Formation; Samples with "*" were quoted from Shi (2017).

0.74 to 1.09). The mean value of δCe of the D-2 reservoir bitumen is 1.09 (ranging from 0.78 to 2.16), and the mean value of δPr is 0.85 (ranging from 0.59 to 1.04). The mean value of δCe of the LWM reservoir bitumen is 1.05 (ranging from 0.80 to 1.53), and the mean value of δPr is 0.90 (ranging from 0.76 to 1.02). Except two D-4 reservoir bitumen samples fall on the top of area V, showing a weakly negative Ce anomaly, the other bitumen samples all fall in the areas outside of area V, indicating that there is almost no negative Ce anomaly in the reservoir bitumen (Fig. 4).

5. Discussion

5.1. Differences in source rocks

The D-3 Member in the central Sichuan Basin was mainly shallow-water shelf facies, while the QZS Formation was mainly deep-water shelf facies (Hou et al., 2017). The difference in depositional facies indicates differences in the depositional environment and provenance of the two sets of source rocks, laying an essential foundation for the gas-source correlation.

5.1.1. Differences in depositional environment

V and Ni belong to the iron group elements, and their ions often present different ion valences under different redox conditions. V is readily adsorbed under reducing conditions, while Ni is easily enriched under reducing conditions. The V/(V + Ni) ratio is often used to distinguish the depositional environment of source rocks (Jones and Manning, 1994; Rimmer, 2004). Generally, a V/(V + Ni) ratio less than 0.46 indicates an anoxic depositional environment, from 0.46 to 0.60 indicates a dysoxic depositional environment, from 0.60 to 0.82 indicates an anoxic depositional environment, and greater than 0.82 indicates a euxinic depositional environment (Jones and Manning, 1994; Rimmer, 2004). The V/(V + Ni) ratio of the QZS source rock in the study area ranges from 0.57 to 0.88 (mean value of 0.69). Except for one sample in the dysoxic area, the other samples are distributed in the anoxic area. The V/(V + Ni) ratio of the D-3 source rock ranges from 0.44 to 0.64 (mean value of 0.56). Only three samples fall in the anoxic area, and the rest are distributed in the dysoxic area (Fig. 5).

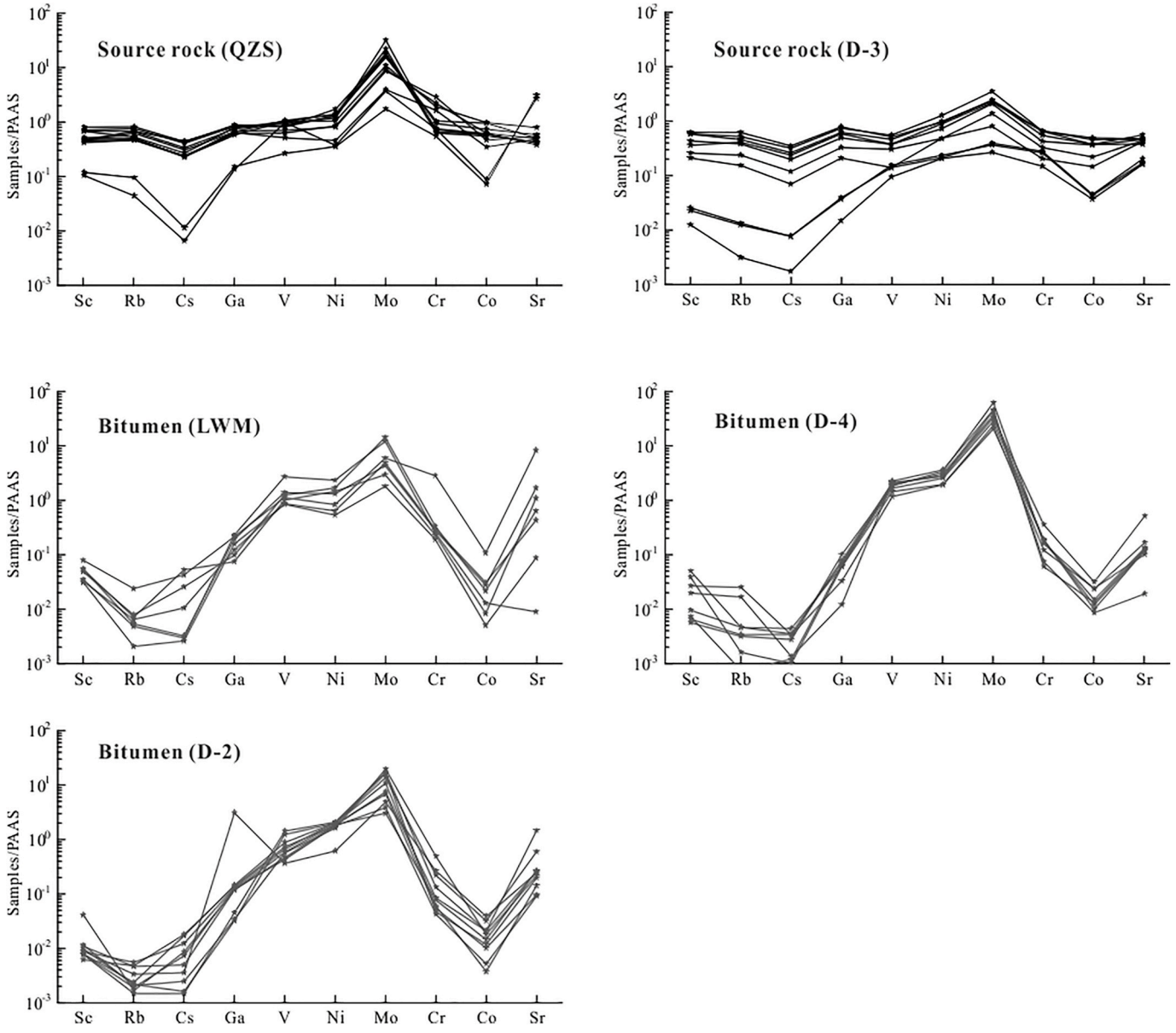

Fig. 3. Distribution pattern of trace elements in source rocks and reservoir bitumen in the study area (PAAS-normalized).
The QZS source rock samples show more obvious positive Mo anomalies than the D-3 source rock compared with adjacent elements. The three types of reservoir bitumen also show apparent positive Mo anomalies, showing a higher similarity to the QZS source rock.

Studies have shown that as the HS^- concentration rises from 10^{-4} M to 10^{-3} M in an anoxic environment, MoO_4^{2-} suddenly transforms into MoS_4^{2-}, which is absorbed into sediments by iron oxides or humus (Dean et al., 1997). Subsequently, MoS_4^{2-} transforms into MoS_2 precipitation or enters pyrite as a solid solution, resulting in the enrichment of Mo in sediments in an anoxic environment (Algeo and Maynard, 2004). Therefore, Mo/Ni ratio is often used to identify the depositional environment (Akinlua et al., 2010). The greater the Mo/Ni ratio is, the more reducing the depositional environment is. The Mo/Ni ratio of the QZS source rock has a mean value of 0.23 (ranging from 0.09 to 0.5), while that of the D-3 source rock has a mean value of only 0.04 (ranging from 0.02 to 0.05), indicating that the depositional environment of QZS source rock is more reducing (Fig. 6).

The trivalent REE enters the carbonate minerals to replace the Ca^{2+} in the crystal lattice with the isomorphism or enters the carbonate minerals through adsorption or complexation. REE only slightly differentiates when entering sediments from ocean bottom water through this way, but the difference in redox environment can cause significant differentiation and cause Ce anomaly (Bellanca et al., 1997). In oxygen-enriched seawater, Ce^{3+} is oxidised to Ce^{4+}, and Ce^{4+} is hydrolysed to form highly insoluble $Ce(OH)_4$, resulting in the separation of Ce from La and Pr and negative Ce anomaly. There is no significant difference between Ce^{3+} and other trivalent REE in anoxic seawater, resulting in no negative Ce anomaly or slight positive Ce anomaly. The highly insoluble Ce^{4+} compound will be reduced to soluble Ce^{3+} when it enters the deep-sea reducing environment and re-enters the water body. Therefore, the Ce anomaly in seawater has a good relationship with the redox environment (German and Elderfield, 1990).

In Fig. 4, most of the QZS source rock samples are distributed in the areas I and II, showing no Ce anomaly (Fig. 4), indicating that the QZS source rock was deposited in a relatively reducing environment. While the D-3 source rock samples are all distributed in area V, showing a negative Ce anomaly, indicating a more oxic depositional environment of the D-3 Member. In addition, the Ce anomaly index (Ce_{anom}) can also be used as an effective parameter for analysing source rock depositional

Table 2
Rare earth element composition of source rock and solid bitumen, central Sichuan Basin.

Samples	La	Ce	Pr	Nd	Sm	Eu	Gd	Tb	Dy	Ho	Er	Tm	Yb	Lu	Y	REE + Y	L/H	δEu	δCe	δPr
	μg/g																			
ZJ2-1R	26.30	52.80	6.24	22.80	4.36	0.83	3.15	0.54	2.93	0.45	1.24	0.20	0.97	0.11	13.00	135.92	1.08	1.06	0.95	1.06
ZJ2-2R	8.49	24.10	3.71	18.40	4.01	0.81	3.12	0.60	2.90	0.47	1.45	0.16	1.11	0.10	12.10	81.53	0.73	1.07	0.94	0.99
ZJ2-3R	7.97	20.10	3.31	18.00	4.53	1.02	3.34	0.64	3.87	0.60	1.42	0.14	1.17	0.12	15.00	81.23	0.69	1.23	0.87	0.96
ZJ2-4R	14.50	25.40	3.83	16.60	4.22	0.85	3.06	0.58	3.03	0.45	1.32	0.17	1.12	0.14	14.30	89.57	0.77	1.11	0.78	1.07
PT1-1R	67.40	51.90	13.30	61.10	11.60	2.49	12.10	2.48	14.70	3.30	10.30	1.31	7.43	0.88	148.00	408.29	0.43	0.98	0.40	1.23
PT1-2R	73.70	42.00	18.60	86.80	18.20	3.82	19.00	3.79	24.10	5.17	15.00	1.82	9.92	1.22	206.00	529.14	0.39	0.96	0.26	1.36
PT1-3R	11.20	29.80	3.74	17.10	4.32	0.75	3.16	0.54	2.64	0.45	1.42	0.15	1.08	0.12	12.90	89.37	0.78	0.95	1.04	0.96
PT1-4R	16.50	37.60	5.41	23.60	4.75	0.98	3.15	0.61	2.95	0.51	1.34	0.18	1.23	0.14	13.60	112.55	0.93	1.19	0.90	1.05
AP1-1R*	38.00	72.00	8.20	31.00	4.90	0.93	4.30	0.77	4.70	0.98	2.83	0.42	2.74	0.41	26.20	198.38	0.70	0.95	0.94	1.02
AP1-2R*	26.70	50.00	5.70	22.00	4.50	0.84	4.10	0.71	4.40	0.92	2.60	0.39	2.51	0.38	23.80	149.55	0.58	0.92	0.93	1.01
AP1-3R*	35.00	70.00	8.20	33.00	5.70	1.02	5.00	0.87	5.40	1.11	3.20	0.47	3.10	0.47	28.60	201.14	0.63	0.90	0.95	1.00
AP1-4R*	38.00	67.00	7.40	25.40	3.90	0.67	3.50	0.63	4.00	0.88	2.68	0.41	2.79	0.43	22.80	180.49	0.66	0.85	0.92	1.05
GK1-1R	4.45	2.72	0.90	4.23	0.75	0.19	0.76	0.13	0.73	0.13	0.38	0.06	0.33	0.04	5.40	21.19	0.64	1.20	0.31	1.28
GK1-2R	10.20	6.12	1.83	8.71	1.42	0.30	1.41	0.24	1.20	0.22	0.70	0.07	0.38	0.05	8.07	40.90	0.77	0.98	0.32	1.24
GK1-3R	6.66	3.50	1.06	4.93	0.83	0.17	0.73	0.12	0.63	0.12	0.29	0.03	0.20	0.04	3.58	22.89	0.88	1.04	0.30	1.27
GK1-4R	46.60	41.80	8.99	39.60	6.89	1.42	6.73	1.17	6.67	1.29	3.40	0.41	2.08	0.29	45.40	212.73	0.70	0.98	0.47	1.20
GK1-5R	31.40	26.60	6.03	26.40	4.82	1.00	4.13	0.72	3.72	0.67	1.91	0.22	1.32	0.14	25.70	134.78	0.83	1.06	0.44	1.23
GK1-1R*	71.00	60.00	12.80	58.00	10.20	1.91	9.50	1.48	8.70	1.80	4.90	0.64	3.80	0.57	58.00	303.30	0.69	0.91	0.46	1.18
GK1-2R*	60.00	54.00	10.70	47.00	8.50	1.62	8.50	1.37	8.30	1.76	4.80	0.64	3.70	0.55	56.00	267.44	0.61	0.89	0.49	1.17
GK1-3R*	62.00	58.00	10.80	48.00	8.60	1.59	8.30	1.30	7.90	1.65	4.40	0.59	3.60	0.54	52.00	269.27	0.65	0.88	0.51	1.14
GK1-4R*	23.10	22.50	4.70	22.60	4.10	0.84	3.90	0.60	3.50	0.73	1.83	0.23	1.27	0.18	25.00	115.08	0.70	0.99	0.50	1.12
GK1-5R*	48.00	43.00	8.50	38.00	6.90	1.37	6.70	1.07	6.40	1.34	3.60	0.48	2.82	0.42	41.00	209.60	0.64	0.95	0.49	1.16
MX39-1B	0.17	0.25	0.03	0.16	0.03	0.01	0.03	0.01	0.02	0.01	0.01	0.00	0.01	0.00	0.12	0.84	0.77	1.29	0.86	0.74
MX39-2B	0.16	0.27	0.03	0.13	0.02	0.01	0.03	0.00	0.01	0.00	0.01	0.00	0.02	0.01	0.10	0.78	0.55	1.43	0.91	0.91
MX39-3B	0.23	0.48	0.05	0.20	0.06	0.02	0.05	0.00	0.03	0.01	0.02	0.00	0.02	0.00	0.23	1.38	0.98	1.31	1.10	0.84
MX39-4B	0.03	0.07	0.01	0.02	0.01	0.00	0.01	0.00	0.01	0.00	0.01	0.00	0.00	0.01	0.08	0.26	0.27	1.47	1.19	0.87
MX116-1B	0.89	1.00	0.11	0.43	0.10	0.03	0.12	0.01	0.03	0.01	0.02	0.01	0.21	0.06	0.41	3.43	0.33	1.23	0.71	0.96
MX125-1B	0.14	0.31	0.04	0.16	0.05	0.01	0.04	0.01	0.03	0.01	0.02	0.01	0.14	0.04	0.27	1.24	0.17	1.04	1.02	0.93
GK1-1B*	1.36	2.25	0.43	2.13	0.47	0.12	0.43	0.07	0.33	0.06	0.15	0.02	0.07	0.01	1.97	9.87	0.81	1.23	0.67	1.07
AP1-1B*	0.17	0.35	0.05	0.19	0.03	0.02	0.04	0.00	0.02	0.00	0.01	0.00	0.01	0.00	0.20	1.09	1.28	2.20	0.88	1.09
PT1-1B	2.20	2.66	0.23	0.97	0.16	0.05	0.17	0.01	0.05	0.00	0.02	0.01	0.02	0.01	0.37	6.92	1.99	1.43	0.80	0.85
PT1-2B	1.81	2.22	0.19	0.66	0.09	0.01	0.07	0.01	0.01	0.00	0.01	0.00	0.01	0.01	0.17	5.26	2.87	0.85	0.81	0.92
PT1-3B	0.72	1.14	0.12	0.47	0.11	0.03	0.10	0.01	0.08	0.02	0.06	0.01	0.08	0.01	0.71	3.66	0.64	1.50	0.90	0.93
PT1-4B	0.78	1.01	0.11	0.39	0.09	0.02	0.09	0.01	0.05	0.01	0.02	0.01	0.01	0.01	0.32	2.93	1.09	1.24	0.78	1.01
ZJ2-1B	0.12	0.30	0.02	0.09	0.01	0.00	0.02	0.00	0.01	0.01	0.01	0.00	0.02	0.01	0.08	0.68	0.33	1.53	1.49	0.62
ZJ2-2B	0.22	0.51	0.05	0.14	0.06	0.01	0.04	0.01	0.03	0.01	0.02	0.01	0.04	0.02	0.15	1.30	0.35	0.79	1.15	1.04
ZJ2-3B	0.81	1.18	0.10	0.59	0.19	0.06	0.19	0.01	0.05	0.01	0.03	0.02	0.29	0.09	0.65	4.26	0.33	1.38	0.92	0.68
ZJ2-4B	0.31	0.58	0.06	0.21	0.04	0.01	0.04	0.01	0.04	0.01	0.02	0.01	0.04	0.01	0.25	1.63	0.48	1.19	0.96	1.03
ZJ2-5B	0.20	0.35	0.04	0.20	0.04	0.01	0.04	0.00	0.02	0.01	0.01	0.01	0.02	0.01	0.18	1.13	0.55	1.33	0.92	0.84
ZJ2-6B	0.07	0.27	0.01	0.04	0.02	0.01	0.02	0.00	0.01	0.00	0.00	0.00	0.10	0.03	0.07	0.64	0.12	1.41	2.16	0.59
LT1-1B	0.20	0.35	0.04	0.15	0.03	0.01	0.02	0.01	0.02	0.01	0.01	0.01	0.21	0.06	0.08	1.17	0.13	1.24	0.90	1.02
LT1-2B	0.32	0.59	0.05	0.18	0.05	0.02	0.05	0.00	0.02	0.01	0.02	0.00	0.09	0.03	0.20	1.64	0.35	1.50	1.05	0.91
MX26-1B	0.10	0.29	0.02	0.07	0.01	0.01	0.01	0.00	0.01	0.00	0.00	0.01	0.13	0.06	0.07	0.78	0.08	2.12	1.53	0.76
MX26-2B	0.43	0.98	0.08	0.35	0.09	0.02	0.06	0.01	0.08	0.01	0.04	0.01	0.15	0.04	0.12	2.46	0.29	1.07	1.22	0.77
MX26-3B	3.41	5.18	0.62	3.02	0.71	0.21	0.78	0.08	0.47	0.08	0.25	0.07	0.92	0.26	3.39	19.43	0.39	1.30	0.82	0.91
MX56-1B	2.00	2.51	0.23	0.80	0.14	0.03	0.11	0.02	0.08	0.01	0.06	0.01	0.26	0.10	0.42	6.77	0.43	1.25	0.80	0.95

Note: $\delta Eu = 2Eu_{SN}/(La_{SN} + Pr_{SN})$, $\delta Ce = 2Ce_{SN}/(Sm_{SN} + Gd_{SN})$, $\delta Pr = 2Pr_{SN}/(Ce_{SN} + Nd_{SN})$, SN means that the data was normalized by Post-Archean Australian Shale (PAAS); L/H means the ratio of light REE and heavy REE; Samples with "*" are quoted from Shi (2017).

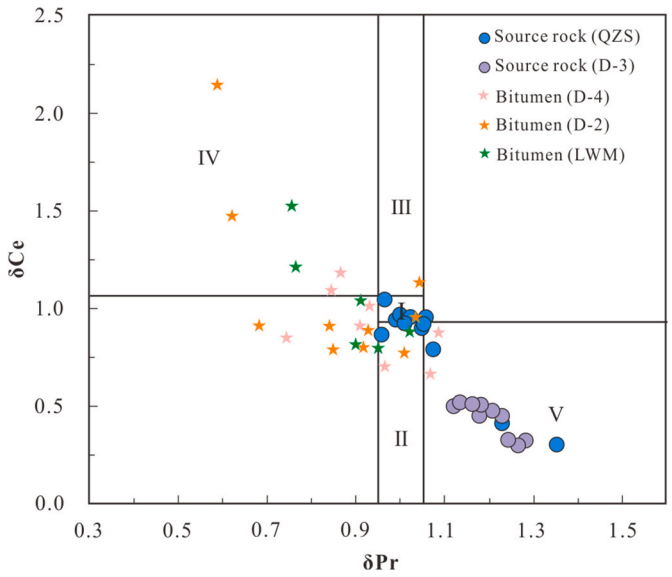

Fig. 4. The Ce anomaly identification chart in the source rock and reservoir bitumen (according to Bau and Dulski, 1996).
In the figure, all of the samples from the source rock of the D-3 Member are distributed in area V, indicating the true negative Ce anomaly. The samples from the QZS source rock are mainly distributed in areas I and II, and a few are distributed in area V, indicating that most of the samples do not show Ce anomaly, and only a few samples show negative Ce anomaly. Most of the reservoir bitumen samples of the D-4 Member, D-2 Member, and LWM Formation are distributed outside of area V, showing no negative Ce anomaly. Two bitumen samples from the D-4 Member are distributed at the top of area V, showing a weakly negative Ce anomaly.

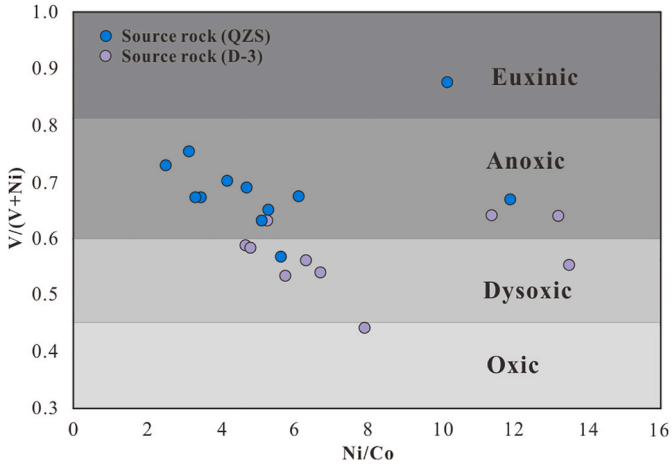

Fig. 5. Ni/Co versus V/(V + Ni) cross plot of QZS and D-3 source rocks.
Except for two samples from the QZS source rock located in the dysoxic and euxinic area, the rest located in the anoxic area, reflecting that the QZS source rock was mainly deposited in an anoxic environment. Except for three samples from the D-3 source rock fall in the anoxic area, most samples fall in the dysoxic area, indicating that the D-3 Member rock was mainly deposited in the dysoxic environment.

environment. Ce anomaly index (Ce_{anom}) is used to express the relative changes between Ce, La and Nd, and the calculation formula is $Ce_{anom} = Lg[3*Ce_{SN}/(2*La_{SN} + Nd_{SN})]$ (Eiderfield et al., 1982). When $Ce_{anom} >$ -0.1, indicates the enrichment of Ce, reflecting the anoxic depositional environment, while $Ce_{anom} < -0.1$, indicates the depletion of Ce, reflecting the oxic depositional environment (Raiswell and Buckley, 1988; Deng and Qian, 1993). Fig. 6 shows that the Ce_{anom} of the D-3 source rock samples are all less than −0.1, indicating an oxic

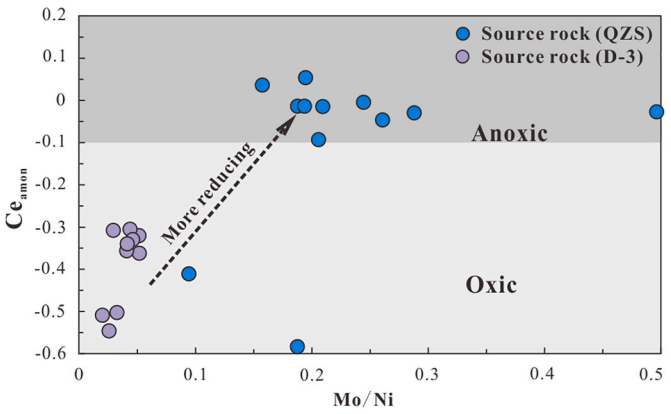

Fig. 6. Mo/Ni versus Ce_{anom} cross plot of the QZS and D-3 source rocks.
The Ce_{anom} and Mo/Ni values of the QZS source rock are greater than those of the D-3 source rock. Except for two samples from the QZS Formation falling in the oxic area, the rest samples from the QZS Formation fall in the anoxic area, indicating that the QZS source rock was mainly deposited in an anoxic environment. All samples from the D-3 Member are located in the oxic area, showing the characteristics of the oxic depositional environment.

depositional environment, while Ce_{anom} values of the QZS source rock samples are mainly greater than −0.1, indicating an anoxic depositional environment (Fig. 6).

On the whole, compared with the D-3 source rock, the QZS source rock was mainly deposited in an anoxic environment, and the depositional environment was more reducing, which is consistent with the previous study of depositional facies (Hou et al., 2017). The QZS Formation was mainly deposited in deep-water shelf facies, while the D-3 Member was mainly deposited in shallow-water shelf facies. During the deposition of the QZS Formation, the seawater was deeper, and the depositional environment was more anoxic than the D-3 source rock.

5.1.2. *Differences in provenance*

Studies have shown that the concentration of V and Ni can reflect the depositional environment of sedimentary rocks to a certain extent (Lewan and Maynard, 1982; Lewan, 1984; Galarraga et al., 2008; Akinlua et al., 2010) (Fig. 7). Fig. 7 shows that the D-3 source rock samples all fall in the terrestrial area, representing the significant influence of terrestrial materials during the deposition of the D-3 Member, while the QZS source rock is different, with more supply of marine

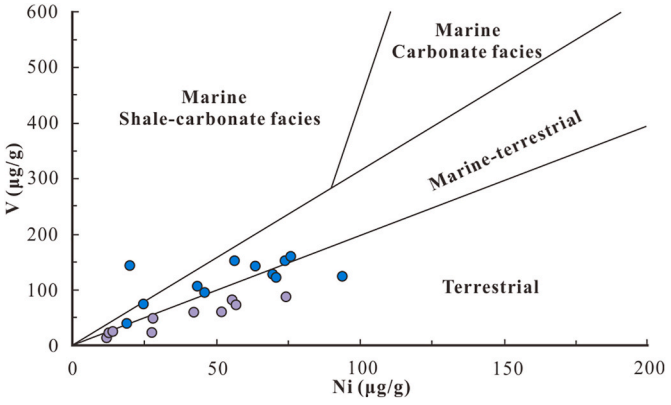

Fig. 7. Ni versus V cross plot of the QZS and D-3 source rocks (The chart was quoted from Galarraga et al., 2008; Akinlua et al., 2010).
All samples from the D-3 source rock fall in the terrestrial area, indicating that the supply of terrestrial materials was significant. For the QZS source rock, except for a few samples that fall in the terrestrial area, most of the samples fall in the marine-terrestrial area, indicating the supply of both marine and terrestrial materials.

materials.

Elements such as Co and Sc are mainly controlled by terrestrial sources and are not sensitive to redox-insensitive environments, which are often used in provenance analysis (Liu et al., 1987; Algeo, 2004). The La/Sc and La/Co ratios are often used to analyse the provenance of sedimentary rocks. When La/Sc value ranges from 2.5 to 16.3, the source rock is mainly felsic, while La/Sc value ranges from 0.43 to 0.86, the source rock is mainly mafic (Cullers, 2000). La/Co value shows a similar characteristic; when the La/Co value ranges from 1.8 to 13.8 or from 0.14 to 0.38, the source rock is mainly felsic or mafic, respectively (Cullers, 2000). The source rocks' La/Co and La/Sc ratios indicate that the QZS and D-3 source rocks are significantly different in provenance. The La/Co value of the D-3 source rock ranges from 5.1 to 9.4, and La/Sc value ranges from 5.9 to 24.0, indicating that the provenance was mainly felsic (Fig. 8). The La/Co value of the QZS source rock mainly ranges from 0.4 to 2.8, and La/Sc value mainly ranges from 1.1 to 5.1, showing more mafic provenance characteristics (Fig. 8). It is consistent with the depositional environment restored by V and Ni and the study of previous depositional facies. The D-3 source rock was mainly deposited in shallow-water shelf facies close to the terrestrial source and deposited more felsic terrestrial materials. The QZS source rock was mainly deposited in deep-water shelf facies, which was farther away from the terrestrial sources than the D-3 Member, and the contribution of marine materials is obviously more significant, showing more enriched mafic provenance.

5.2. Reservoir bitumen-source rock correlation

5.2.1. Distribution pattern

The REE distribution curve of the QZS source rock is relatively flat, showing a slight enrichment of heavy REE (L/H, mean value of 0.7), with no apparent Ce anomaly (δCe, mean value of 0.82 and no Eu anomaly (δEu, mean value of 1.02). The REE distribution curve of the D-3 source rock is relatively flat, showing a slight enrichment of heavy REE (L/H, mean value of 0.7), with apparent negative Ce anomaly and no Eu anomaly (δEu, mean value of 0.99) (Fig. 9).

The D-4, D-2, and LWM reservoir bitumen have similar REE distribution patterns, which is different from the D-3 source rock and is more similar to the QZS source rock. According to the REE distribution model, the bitumen in the three reservoirs can be subdivided into two categories: "flat, no Ce anomaly" and "upturned tail, no Ce anomaly". Compared with the first category, the second category shows an apparent upturned tail. Previous studies show that some dumbbell-shaped barites were observed in the pores of the bitumen in the DY Formation reservoir (Gao, 2016). These barites are believed to be of hydrothermal origin (Gao, 2016). Hydrothermal minerals can usually show the enrichment of heavy REE and the depletion of light REE (Sun et al., 2014). These heavy REE enriched barites filled in the solid bitumen pores are mixed with bitumen powder during the sample preparation process. To a certain extent, some heavy REE (Tm, Yb, Lu, etc.) in the bitumen sample were enriched, which caused the upturned tail of the bitumen REE distribution curve. It is worth noting that, these bitumen samples with upturned tails usually showed a certain degree of positive Eu anomaly, while the positive Eu anomaly in the bitumen of the DY Formation was also explained as the hydrothermal origin (Gao et al., 2017), further confirming that the hydrothermal fluid causes the enrichment of some heavy REE in the bitumen.

Overall, the REE distribution curves of most bitumen samples show substantial similarity to that of the source rocks, and the bitumen samples only show slight Eu anomalies. In addition, the proportion of hydrothermal minerals, like barite, in the bitumen pores is very limited (Gao, 2016), which can only affect the concentration of some heavy REE. So, The REE transformation in the bitumen by hydrothermal activities is very limited. To ensure the reliability of study results, the influenced REE was not used in the study.

5.2.2. Provenance parameters correlation

The La/Co and the La/Sc values of the D-4 reservoir bitumen and LWM reservoir bitumen are located in the range of (0.2, 4.1) and (0.2, 3.2), respectively. It indicates that the source of the D-4 and LWM reservoir bitumens were mainly mafic, which is very similar to the QZS source rock. It demonstrates that the D-4 and LWM reservoir bitumens were derived from the QZS source rock (Fig. 10). In contrast, the D-2 reservoir bitumen shows a significantly larger range span, with La/Co value ranging from 0.7 to 3.7, La/Sc value ranging from 0.3 to 14.8 (Fig. 10). Although most of the samples are similar to the QZS source rock, the samples named PT1-1B and PT1-2B show prominent felsic characteristics, distributed in the transition zone between the D-3 Member and QZS Formation, close to the D-3 Member. It indicates that the D-3 source rock was the primary source of the two bitumen samples (Fig. 10). According to the analysis of provenance parameters, the D-4 reservoir bitumen and LWM reservoir bitumen were mainly derived from the QZS source rock, while the D-2 reservoir bitumen had prominent source characteristics of the D-3 source rock.

5.2.3. Redox parameters correlation

(a) *Rare earth elements*

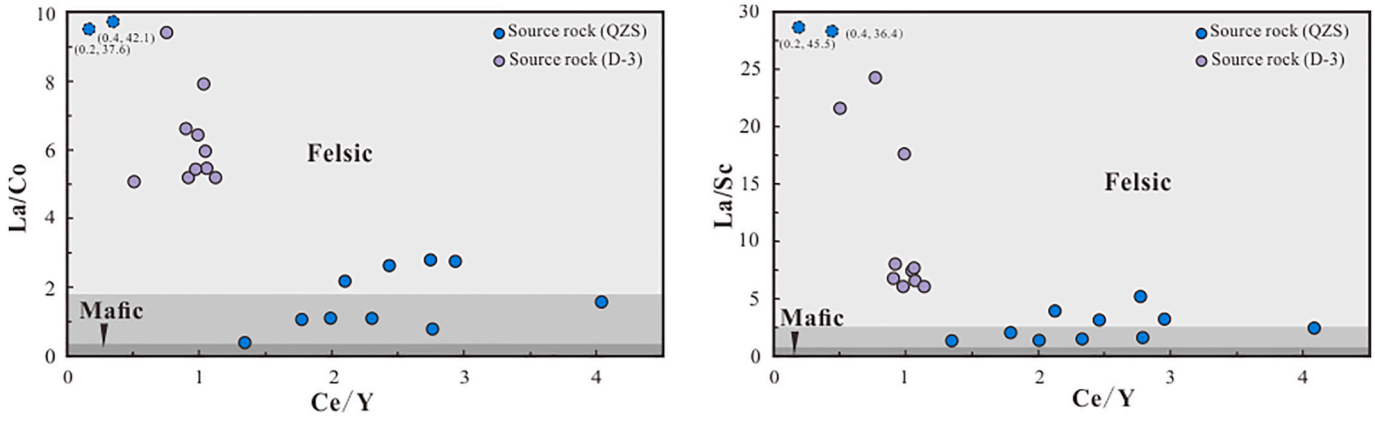

Fig. 8. Elements cross plot of the QZS and D-3 source rocks.
For the D-3 source rock, the La/Co value is greater than 1.8, and the La/Sc value is greater than 2.5, indicating that the D-3 source rock was dominated by felsic. For the QZS source rock, except for the two samples named PT1-1R and PT1-2R, whose primary source was felsic (the blue dot in the upper left corner of the figure), the La/Co value of the rest of the samples mainly ranges from 0.4 to 2.8, and La/Sc value mainly ranges from 1.1 to 5.1, indicating that the provenance was mainly a mixture of felsic and mafic.

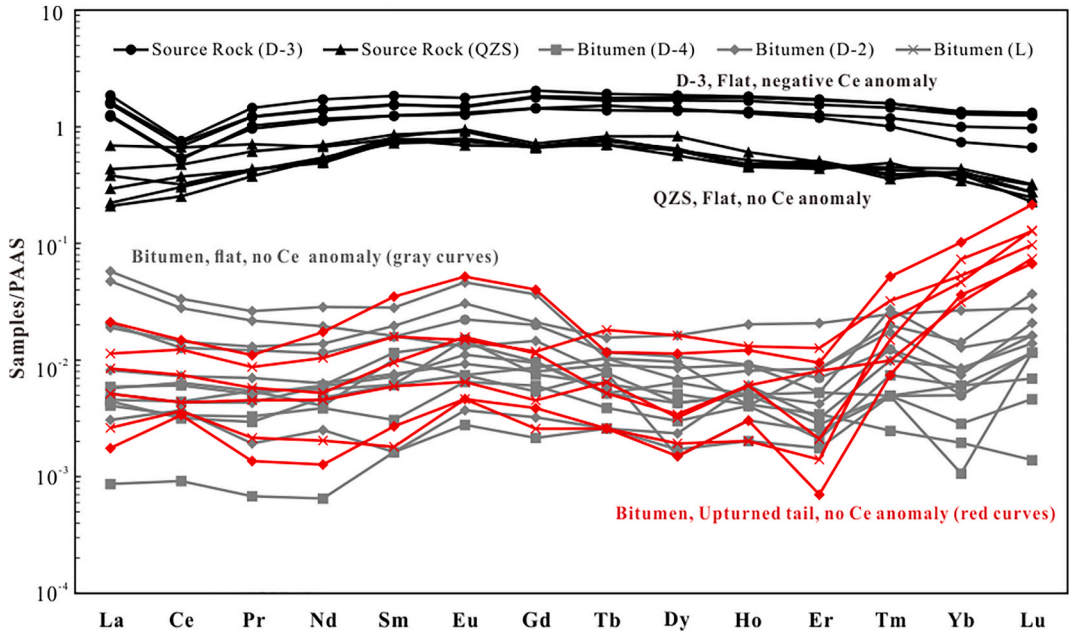

Fig. 9. Distribution pattern of REE in the source rocks and reservoir bitumen.
The REE distribution curves of the QZS and D-3 Member are flat and show a slight enrichment of heavy REE (L/H, mean value of 0.7). In addition, the D-3 source rock shows a negative Ce anomaly, while the QZS source rock shows no Ce anomaly. Most of the REE distribution curves of the bitumen from the D-4 Member, D-2 Member, and LWM Formation are flat, and no negative Ce anomaly. The rest of the REE distribution curves have upturned tails, slightly positive Eu anomaly, and no negative Ce anomaly.

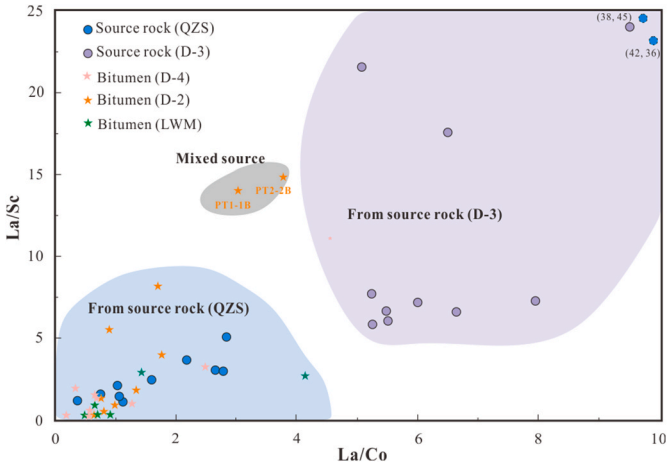

Fig. 10. La/Co versus La/Sc cross plot of the reservoir bitumen and source rocks in the study area.
The distribution range of D-4 reservoir bitumen and LWM reservoir bitumen coincides with the QZS source rock, indicating that the reservoir bitumen was derived from the QZS source rock. The distribution range of D-2 reservoir bitumen is extensive; the samples named PT1-1B and PT1-2B fall in the transition zone between D-3 Member and QZS source rocks, indicating mixed source characteristics.

In Fig. 4, the QZS source rock samples mainly fall in area I, exhibiting no Ce anomalies and representing a reducing depositional environment (Figs. 4 and 6). The D-3 source rock samples are all located in area V, showing true negative Ce anomalies, and representing a more oxic depositional environment (Figs. 4 and 6). The D-2, D-4 and LWM reservoir bitumens show no negative Ce anomalies. The δCe values of some bitumen samples are slightly lower than 1, mainly due to the false Ce anomaly caused by the enrichment of La, which indicates that the source rock of the reservoir bitumen was mainly deposited in the reducing environment, showing similarity with the QZS source rock. δCe and Ce/Y parameters can effectively distinguish the source rocks from different depositional environments (Gao et al., 2016; Shi, 2017). Fig. 11 shows that the D-4 Member, D-2 Member and LWM reservoir bitumen samples all fall within the distribution range of the QZS source rock, while almost no samples fall within the range of the D-3 source rock, indicating that the reservoir bitumen of the three strata was closely related to the QZS source rock (Fig. 11).

(b) *Trace elements*

The prerequisite of using trace elements for hydrocarbon and source correlation is that external trace elements had not significantly modified the crude oil during the migration process and the later alteration

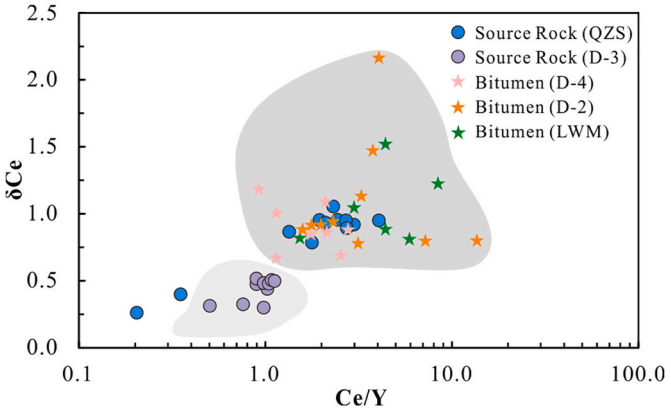

Fig. 11. Intersection diagram of δCe and Ce/Y of source rock and reservoir bitumen.
All reservoir bitumen samples of the D-4 Member, D-2 Member and LWM Formation fall within the distribution range of the QZS source rock and have no overlap with the distribution range of D-3 source rock, indicating that the solid bitumen in the three sets of reservoirs was closely related to the QZS source rock.

process in the reservoir. The solubility of different valence ions of elements such as V and Mo in seawater is different, which is easy to cause differentiation and reflect in the sediments (Jones and Manning, 1994; Tribovilard et al., 2006). V and Mo elements are usually highly enriched in anoxic sediments but not in oxic sediments (Rimmer, 2004; Tribovilard et al., 2006). In the D-3 Member and QZS source rocks, the V and Ni elements have a reasonable correlation, representing a similar enrichment law during the depositional period (Fig. 12). Although the concentration of V and Ni of the reservoir bitumen had been changed during migration of crude oil or the alteration in the reservoir, the reservoir bitumen inherited the characteristic synergistic change between V and Mo elements of the source rock, in particular, showing the similarity with the QZS source rock (Fig. 12). Therefore, V and Ni elements can be used to study the redox characteristics of the source of the reservoir bitumen (Jones and Manning, 1994; Morford and Emerson, 1999; Sarkar et al., 2003; Algeo and Maynard, 2004; Tribovilard et al., 2006; Lin et al., 2008).

The V/(V + Ni) value of LWM reservoir bitumen ranges from 0.67 to 0.81 (mean value of 0.76), and the Mo/Ni value ranges from 0.06 to 0.16 (mean value of 0.11). It indicates that the source rock was deposited in an anoxic environment, consistent with the QZS source rock, reflecting that the LWM reservoir bitumen was mainly derived from the QZS source rock (Fig. 13). Similar to the LWM reservoir bitumen, the V/(V + Ni) value of the D-4 reservoir bitumen ranges from 0.60 to 0.67 (mean value of 0.64), and the Mo/Ni value ranges from 0.19 to 0.33 (mean value of 0.24), representing an anoxic environment of the source rock, showing consistency with the QZS source rock (Fig. 13). The source characteristics of D-2 reservoir bitumen are different. The V/(V + Ni) value ranges from 0.40 to 0.65 (mean value of 0.52), Mo/Ni value ranges from 0.03 to 0.22 (mean value of 0.11), and the span range is larger (Fig. 13). Although some bitumen samples show anoxic sources consistent with the QZS source rock, the samples named ZJ2-2B and ZJ2-1B show more oxic source characteristics, which are more consistent with the D-3 source rock (Fig. 13). This result is consistent with the results obtained by La/Sc and La/Co analysis. In addition, samples named ZJ2-3B and ZJ2-4B are distributed in the transition zone between the two sets of source rocks, showing the characteristics of mixed sources. According to the comprehensive correlation results, the LWM reservoir bitumen and D-4 reservoir bitumen were derived from the QZS source rock. At the same time, the D-2 reservoir bitumen was derived both from the QZS and D-3 source rocks.

Further analysis revealed that the four bitumen samples named ZJ2-1B, ZJ2-2B, ZJ2-3B, and ZJ2-4B, with similar characteristics to the D-3 source rock, were all from the top of the D-2 Member reservoir, and the vertical distance to the D-3 source rock (H) is less than 25m, while H of

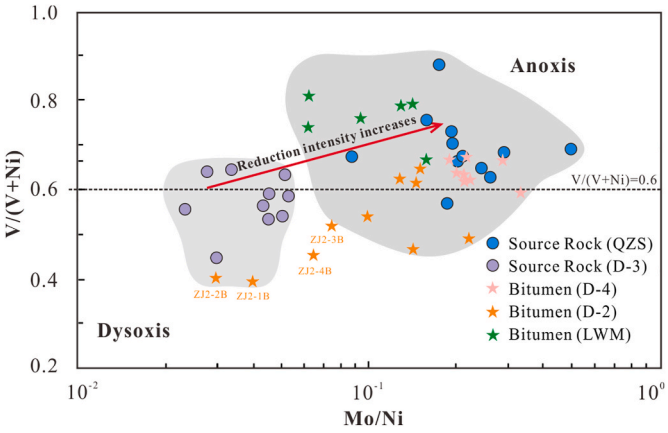

Fig. 13. V/(V + Ni) and Mo/Ni Cross-plot of the source rocks and reservoir bitumen.
The QZS source rock was mainly deposited in an anoxic environment, while the D-3 source rock was mainly deposited in a dysoxic environment. The samples from the LWM reservoir bitumen and D-4 reservoir bitumen fall within the QZS source rock distribution range. Most samples of the D-2 reservoir bitumen fall within the distribution range of the QZS source rock, while two samples named ZJ2-1B and ZJ2-2B fall within the distribution range of D-3 source rock, and two samples named ZJ2-3B、ZJ2-4B fall within the transition zone of two sets of source rocks, indicating that D-2 reservoir bitumen has the contribution of D-3 source rock.

the other bitumen samples derived from the QZS source rock is more than 90m (Figs. 14 and 15). To explore whether the contribution of the D-3 source rock was related to H, all bitumen samples of the underlying D-2 Member and the overlying D-4 Member were analysed. The results show that the contribution of the D-3 source rock has a good correlation with H. When H < 50m, the V/(V + Ni) and Mo/Ni value of the reservoir bitumen are similar to the D-3 source rock, indicating that the reservoir bitumen was mainly derived from the D-3 source rock (Figs. 14 and 15). When H > 50m, with the increase of H, the values of V/(V + Ni) and Mo/Ni gradually increase and become closer to the QZS source rock, indicating that with the increase of H, the contribution of the D-3 source rock is gradually weakened, while the contribution of the QZS source rock is dominant (Figs. 14 and 15). On the whole, in the depth range of 50m above and below the D-3 source rock, the D-3 source rock contributed significantly, while the reservoir is more than 50 m away from the D-3 source rock, the characteristics of the D-3 source rock was almost entirely obscured by QZS source rock (Figs. 14 and 15).

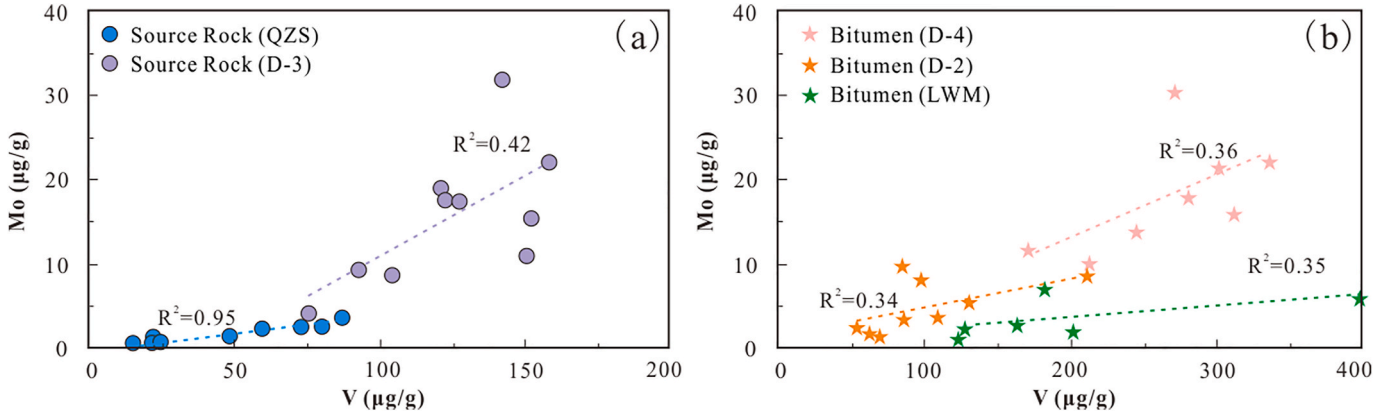

Fig. 12. Mo versus V cross plot of the source rocks and reservoir bitumen.
The Mo and V elements in the QZS and D-3 source rocks show a good positive correlation, and the correlation coefficients are 0.42 and 0.95, respectively. The V and Ni elements in the reservoir bitumen of the D-2 Member, D-4 Member and LWM Formation also show good correlations (correlation coefficients of 0.34, 0.36, and 0.35, respectively), and the correlation coefficients are similar to the QZS source rock.

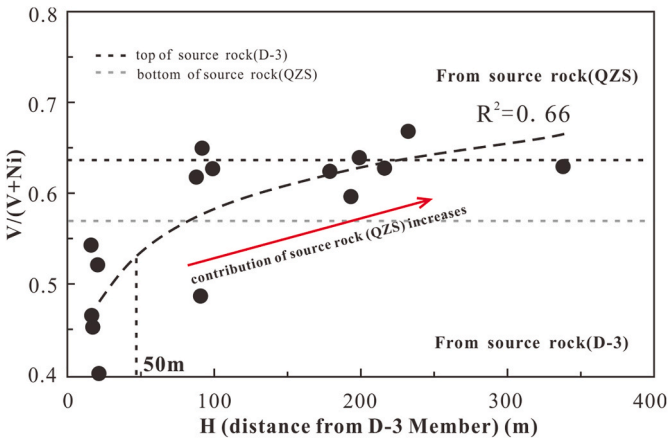

Fig. 14. Cross-plot of V/(V + Ni) ratio in the bitumen from the D-2 Member and D-4 member and the distance from bitumen samples to D-3 source rock (H). V/(V + Ni) ratio has a good fitting relationship with H. With the increase of H, V/(V + Ni) gradually increases, indicating that the contribution of the QZS source rock is gradually increasing. When H < 50 m, the slope of the curve changes significantly, indicating that both the source rocks of the D-3 Member and the QZS Formation contribute. When H > 50m, the slope of the curve changes little, and the curve tends to be stable, indicating that the bitumen mainly derives from the QZS Formation.

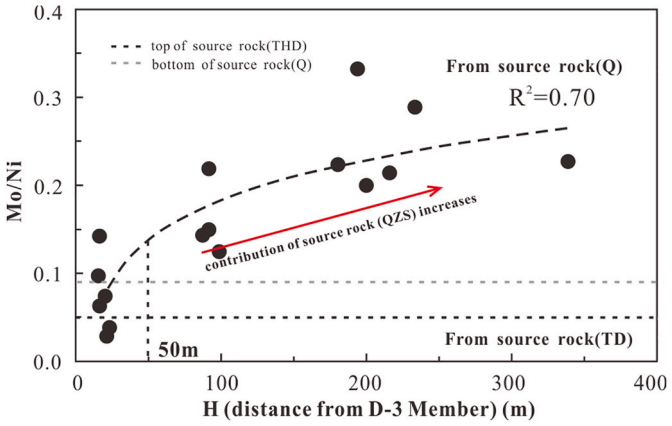

Fig. 15. Cross-plot of Mo/Ni ratio in the bitumen from the D-2 Member and D-4 member and the distance from bitumen samples to D-3 source rock (H). Mo/Ni ratio has a good fitting relationship with H. With the increase of H, Mo/Ni gradually increases, indicating that the contribution of the QZS source rock is gradually increasing. When H < 50 m, the slope of the curve changes significantly, indicating that both the D-3 and QZS source rocks contribute. When H > 50m, the slope of the curve changes little, and the curve tends to be stable, indicating that the bitumen mainly derives from the QZS source rock.

5.3. Crude oil charging mode

The trace elements and REE of the LWM reservoir bitumen indicate that the natural gas was derived from the QZS source rock, consistent with the conclusion obtained by previous organic geochemical correlation methods. It confirmed that the TSR experienced by the natural gas of the LWM Formation was relatively weak, and the organic geochemical information (carbon isotope, biomarkers, etc.) carried by the natural gas and the reservoir bitumen can still indicate the parent source. It can be seen that in highly mature to over mature areas where epigenetic alteration (like TSR) is weak, organic geochemical methods still have specific applicability in gas-source correlation. However, due to the strong TSR on the natural gas of the D-2 and D-4 Members (Wei et al., 2015a; Zhang, 2019; Shuai et al., 2019), the conventional organic geochemical methods for hydrocarbon source correlation are greatly restricted, while trace elements and REE show substantial advantages, which can well distinguish the reservoir bitumen from the two sets of source rocks. Compared with REE, trace element parameters (V/(V + Ni), Mo/Ni) are more sensitive to the reservoir bitumen from different sources, which can better identify the source of the D-3 source rock to the D-2 reservoir bitumen. The contribution of the D-3 source rock was limited to 50 m adjacent to the source rock.

In this study, the D-4 Member bitumen samples did not capture the information of the D-3 source rock, while the D-2 reservoir bitumen showed apparent characteristics of the D-3 source rock, which was related to the crude oil charging process. The crude oil generated from the QZS source rock can enter the D-4 reservoir through lateral and vertical migration (Fig. 16). The vertically migrated crude oil migrated into the D-4 reservoir after a short distance migration and then accumulated in the trap at the top of the D-4 reservoir (Fig. 16). The crude oil migrating laterally into the D-4 reservoir mixed with the vertical migration crude oil from the D-3 Member, then continued to move upwards and finally accumulated in the trap at the top of the D-4 Member (Fig. 16). During this process, the crude oil from the two sets of source rocks was thoroughly mixed, accumulated in the trap at the top of the D-4 Member, and finally, the paleo-oil reservoir formed. The crude oil from the QZS source rock was the primary source, resulting in the complete coverage of the characteristics of the crude oil from the D-3 source rock (Fig. 16), so the characteristics of the D-3 source rock were not found in the reservoir bitumen formed by oil-cracking.

For the D-2 Member reservoir, after the crude oil generated from the D-3 source rock entered the underlying D-2 Member reservoir, it underwent short-distance migration and then accumulated in the trap at the top of the D-2 Member reservoir. The crude oil generated from the QZS source rock mainly migrated laterally into the D-2 Member reservoir (Wu et al., 2016), and finally was trapped, formed paleo-oil reservoir together with the crude oil from the D-3 source rock (Fig. 16). In this process, the crude oil from the D-3 Member did not experience long-distance migration and did not thoroughly mix with the crude oil from the QZS source rock. Therefore, the crude oil in the trap near the D-3 source rock still retains the characteristics of the D-3 source rock, showing obvious "layering" characteristics with the crude oil from the QZS source rock. Because of the large amount of crude oil generated by the QZS source rock, the contribution of the D-3 source rock was limited to a range of 50m near the D-3 Member (Fig. 16). As the distance from the rift trough increased, the difficulty for lateral migration of crude oil generated from the QZS source rock gradually increased. The contribution of the D-3 source rock in the paleo-oil reservoirs would increase. In the internal area of the platform facies, where the crude oil from the QZS source rock was difficult to reach by lateral migration, the D-3 source rock could still provide an effective oil source for the D-2 Member reservoir.

6. Conclusions

The natural gas of the DY Formation is mainly oil-cracking gas. The source of reservoir bitumen is closely related to natural gas. The natural gas of the LWM and DY Formations in the central Sichuan Basin is now in highly-mature to over-mature stages and has experienced strong TSR. The organic geochemical information of the reservoir bitumen and natural gas was significantly changed, limiting the conventional organic geochemical methods in hydrocarbon and source correlation. At the same time, the trace elements and REE provide different insights into gas-source correlation. The differences in the depositional environment of the QZS and D-3 source rocks resulted in the differences in the redox-sensitive elements (V, Mo, etc.) and provenance-sensitive elements (Sc, Co, etc.), laying an essential foundation for gas-source correlation. Through correlation of redox parameters (V/(V + Ni), Mo/Ni, δCe, Ce/Y) and provenance parameters (La/Co, La/Sc), it is concluded that the natural gas of the LWM Formation in the study area was derived from QZS source rock, and had little relationship with the D-3 source rock.

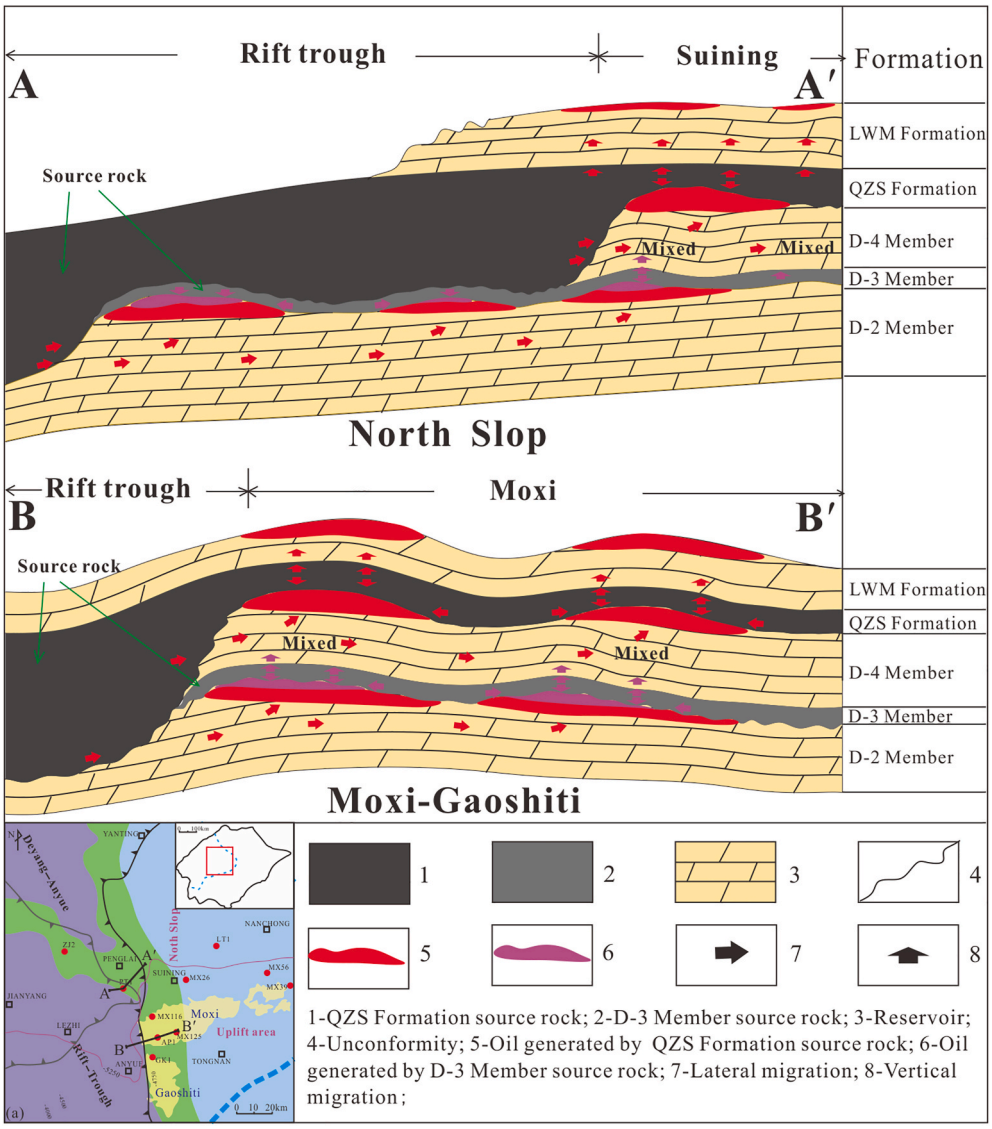

Fig. 16. Crude oil charging mode of D-2 Member, D-4 Member and LWM Formation in the central Sichuan Basin.

The reservoir bitumen of the D-4 and D-2 Members was mainly derived from the QZS source rock, with some contribution of the D-3 source rock. The characteristics of the D-3 source rock in the D-4 reservoir bitumen were obscured by the QZS source rock, while the characteristics of the D-3 source rock remains in the D-2 reservoir bitumen.

The natural gas of the LWM Formation experienced weak TSR, and the results of gas-source correlation by inorganic geochemical methods are consistent with the results of previous correlation using organic geochemical methods. It proves to a certain extent that in highly-mature to the over-mature areas, if TSR or other alterations weakly modified natural gas, organic geochemical methods still have specific applicability in gas-source correlation. As for natural gas altered strongly by TSR or other alterations, the trace elements and REE of reservoir bitumen may provide new insights in gas-source correlation. Therefore, in a brand-new highly-mature area, careful consideration of organic and inorganic geochemistry can be more accurate in hydrocarbon source correlation.

Author contributions

The manuscript was written through the contributions of all authors. All authors have given approval to the final version of the manuscript.

Notes

The authors declare no competing financial interest.

Declaration of competing interest

The authors declare that they have no known competing financial interests or personal relationships that could have appeared to influence the work reported in this paper.

Acknowledgements

This research was financially supported by the National Key R&D Program of China (Grant NO. 2017YFC0603106), the Youth Program of the National Natural Science Foundation of China (Grant NO.41802148). We would also thank the Exploration and Development Research Institute of the Southwest Oil and Gas Field Company PetroChina for providing core samples and necessary data.

References

Akinlua, A., Adekola, S.A., Swakamisa, O., Fadipe, O.A., Akinyemi, S.A., 2010. Trace element characterisation of Cretaceous Orange basin hydrocarbon source rocks. Appl. Geochem. 25, 1587–1595.

Algeo, T.J., 2004. Can marine anoxic events draw down the trace element inventory of seawater? Geology 32, 1057–1060.

Algeo, T.J., Maynard, J.B., 2004. Trace-element behavior and redox facies in core shales of Upper Pennsylvanian Kansas-type cyclothems. Chem. Geol. 206, 289–318.

Bau, M., Dulski, P., 1996. Distribution of yttrium and rare-earth elements in penge and kuruman iron-formations transvaal supergroup South Africa. Precambrian Res. 79, 37–55.

Bellanca, A., Masseti, D., Neri, R., 1997. Rare earth elements in limestone/marlstone couplets from the Albian-Cenomanian Cismon section (Venetian region, northern Italy). Assessing REE sensitivity to environmental changes Chemical Geology 141, 141–152.

Cai, C., Zhang, C., He, H., 2013. Carbon isotope fractionation during methane-dominated TSR in East Sichuan Basin gasfields, China: a review. Mar. Petrol. Geol. 48, 100–110.

Cao, J., Hu, W.X., Yao, S.P., Zhang, Y.J., Wang, X.L., Zhang, Y.Q., Tang, Y., Shi, X.P., 2007. Study on new inorganic geochemical indicators for tracing petroleum migration in Junggar Basin. Science in China (Series D: Earth Sci. 37, 1358–1369.

Cao, J., Hu, W.X., Yao, S.P., Zhang, Y.J., Wang, X.L., Zhang, Y.Q., Tang, Y., Shi, X.P., 2009. Manganese in reservoir calcite cement and its implication for tracing oil migration in Junggar Basin. Acta Pet. Sin. 30, 705–710.

Cao, J., Wu, M., Wang, X.L., Hu, W.X., Xiang, B.L., Sun, P.A., Shi, C.H., Bao, H.J., 2012. Advances in research of using trace elements of crude oil in oil-source correlation. Adv. Earth Sci. 27, 925–936.

Cheng, Y., Hu, Y.Z., Wang, D., Wang, P.P., Li, P.Y., Wang, X.L., 2021. Oil-source rock analysis and metallogenic significance of the palaeo-oil reservoir in the Qinglong antimony deposit, South China. Ore Geol. Rev. 137, 104281.

Connan, J., Lacrampe-Couloume, G., Magot, M., 1995. Origin of Gases in Reservoirs// International Gas Research Conference. Government Insttutes INC, pp. 21–61.

Cullers, R.L., 2000. The geochemistry of shales, siltstones and stones of Pennsylvanian-Permian age, Colorado, USA: implications for provenance and metamorphic studies. Lithos 51, 181–203.

Dai, J.X., Li, J., Luo, X., Zhang, W.Z., Hu, G.Y., Ma, C.H., Guo, J.M., Ge, S.G., 2005. Carbon isotope composition and gas source comparison of alkane gas in the large gas fields of Ordos Basin. Acta Pet. Sin. 18–26.

Dean, W.E., Gardner, J.V., Piper, D.Z., 1997. Inorganic geochemical indicators of glacial-interglacial changes in productivity and anoxia on the California continental margin. Geochem. Cosmochim. Acta 61, 4507–4518.

Deng, H.W., Qian, K., 1993. The Analysis of Sedimentary Geochemistry and Environment. Gansu Science and Technology Press, Lanzhou (in Chinese).

Du, J.H., 2015. Geological Theory and Exploration Practice of Ancient Carbonate Gas Fields. Petroleum Industry Press, Beijing (in Chinese).

Elderfield, H., Greaves, M.J., 1982. The rare earth elements in seawater. Nature 296, 214–219.

Galarraga, F., Llamas, J.F., Martinez, A., Martínez, M., Flamas, J.F., Márquez, G., 2008. V/Ni ratio as a parameter in palaeoenvironmental characterisation of nonmature medium-crude oils from several Latin American basins. J. Petrol. Sci. Eng. 61, 9–14.

Gao, P., 2016. Origin and Source of Sinian Bitumen in the Central Sichuan Basin. China University of Petroleum (Beijing), Doctor's thesis.

Gao, P., Liu, G.D., Jia, C.Z., Young, A., Wang, Z.C., Wang, T.S., Zhang, P.W., Wang, D.P., 2016. Redox variations and organic matter accumulation on the Yangtze carbonate platform during Late Ediacaran–Early Cambrian: constraints from petrology and geochemistry. Palaeogeogr. Palaeoclimatol. Palaeoecol. 450, 91–110.

Gao, P., Liu, G.D., Wang, Z.C., Jia, C.Z., Wang, T.S., Zhang, R.W., 2017. Rareearth dements (REEs) geochemistry of Sinian-Cambrian reservoir solid bitumens in Sichuan Basin, SW China: potential application to petroleum exploration. Geol. J. 52, 298–316.

German, C.R., Elderfield, H., 1990. Application of the Ce anomaly as a paleoredox indicator: the ground rules. Paleoceanography 5, 823–833.

Holman, A.I., Grice, K., Jaraula, C.M.B., Schimmelmann, A., 2014. Bitumen II from the Paleoproterozoic Here's Your Chance Pb/Zn/Ag deposit: implications for the analysis of depositional environment and thermal maturity of hydrothermally-altered sediments. Geochem. Cosmochim. Acta 139, 98–109.

Hou, M.C., Xing, F.C., Xu, S.L., Lin, L.B., Liu, X.C., Xiong, F.H., Huang, H., 2017. Paleogeographical patterns of E-C transition period in the upper Yangtze and the geodynamic mechanism. Acta Sedimentol. Sin. 35, 902–917.

Hou, M.G., Zha, M., Ding, X.J., Yin, H., Bian, B.L., Liu, H.L., Jiang, Z.F., 2021. Source and accumulation process of jurassic biodegraded oil in the eastern junggar basin, NW China. Petrol. Sci. 18, 1033–1046.

Huang, D.F., 1996. Development of hydrocarbon generation theory - (I)Hydrocarnbon generation evolution model of immature oil and organic matter. Adv. Earth Sci. 11, 327–335.

Hunt, J.M., 1996. Petroleum Geochemistry and Geology. W.H. Freeman.

Jones, B., Manning, D., 1994. Comparison of geochemical indices used for the interpretation of palaeoredox conditions in ancient mudstones. Chem. Geol. 111, 111–129.

Lewan, M.D., 1984. Factors controlling the proportionality of vanadium to nickel in crude oils. Geochem. Cosmochim. Acta 48, 2231–2238.

Lewan, M.D., Maynard, J.B., 1982. Factors controlling enrichment of vanadium and nickel in the bitumen of organic sedimentary rocks. Geochem. Cosmochim. Acta 46, 2547–2560.

Li, W., Yi, H.Y., Hu, W.S., 2014. The relationship between the structural evolution of the Caledonian paleo-uplift and hydrocarbon accumulation in the Sichuan Basin. Nat. Gas. Ind. 34, 8–15.

Liang, D.G., Chen, J.P., 2005. Correlation of marine oil sources in high and over-mature areas in South China. Petrol. Explor. Dev. 32, 8–14.

Lin, Z.J., Chen, D.F., Liu, Q., 2008. Geochemical identification indicators for the redox environment of marine sediments. Bulletin of Petrology, Minerals and Geochemistry 27, 72–80.

Liu, Y.J., Cao, L.M., Wang, H.N., 1987. Introduction to Elementary Geochemistry. Geological Publishing House, Beijing (in Chinese).

Ma, K., Zhang, X.H., Peng, H.L., 2020. Tectonic evolution of Moxi north slope in Sichuan Basin and its effect on forming Sinian oil and gas reservoirs. Natural Gas Exploration and Development 43, 8–15.

Ma, Y.S., 2008. Geochemical characteristics and origin of natural gases from Puguang gas field on eastern Sichuan Basin. Natural Gas Geoscience 19, 1–7.

Mankiewicz, P.J., Pottorf, R.J., Kozar, M.G., 2009. Gas geochemistry of the mobile bay jurassic norphlet formation: thermal controls and implications for reservoir connectivity. AAPG (Am. Assoc. Pet. Geol.) Bull. 93, 1319–1346.

Manzano, B.K., Fowler, M.G., Machel, H.G., 1997. The influence of thermochemical sulphate reduction on hydrocarbon composition in Nisku reservoirs, Brazeau river area, Alberta, Canada. Org. Geochem. 27, 507–521.

Mei, L., Zhang, Z.H., Wang, X.D., Yang, Y.C., Liu, L.F., Zhao, Y.D., 2008. Geochemical characteristics and oil source correlation of crude oil in Nanpu Sag, Bohai Bay Basin. Journal of China University of Petroleum (Edition of Natural Science) 32, 40–46.

Mei, Q.H., He, D.F., Wen, Z., 2014. Geological structure and structural evolution of the Leshan-Longnüsi paleo-uplift in the Sichuan Basin. Acta Pet. Sin. 35, 11–25.

Morford, J.L., Emerson, S., 1999. The geochemistry of redox sensitive trace metals in sediments. Geochem. Cosmochim. Acta 63, 1735–1750.

Raiswell, R., Buckley, F., 1988. Degree of pyritisation of iron as a paleoenvironmental indicator of bottom water oxygenation. J. Sediment. Petrol. 58, 812–819.

Ramirez-Caro, D., 2013. Rare Earth Elements (REE) as Geochemical Clues to Reconstruct Hydrocarbon Generation History. Kansas State University, Master's thesis.

Rimmer, S.M., 2004. Geochemical paleoredox indicators in Devonian–Mississippian black shales, central Appalachian Basin (USA). Chem. Geol. 206, 373–391.

Roth, E., Bank, T., Howard, B., Granite, E., 2017. Rare earth elemets in alberta oil sand process streams. Energy Fuels 31, 4714–4720.

Sarkar, A., Sarangi, S., Ebihara, M., Bhattacharya, S.K., Ray, A.K., 2003. Carbonate geochemistry across the Eocene/Oligocene boundary of Kutch, western India: implications to oceanic O_2-poor condition and foraminiferal extinction. Chem. Geol. 201, 281–293.

Shi, C.H., 2017. Applying Inorganic Geochemical Approaches to Conduct Hydrocarbon Source Correlation under Post to Over-mature Conditions: A Case in the Simian and the Lower Cambrian Giant Gas Accumulatiuons, Sichuan, Southwestern China. Nanjing University, Doctor's thesis.

Shi, C.H., Cao, J., Tan, X.C., Luo, B., Zeng, W., Hu, W.X., 2017. Discovery of oil bitumen co-existing with solid bitumen in the Lower Cambrian Longwangmiao giant gas reservoir,Sichuan Basin, southwestern China: implications for hydrocarbon accumulation process. Org. Geochem. 108, 61–81.

Shuai, Y.H., Zhang, S.C., Hu, G.Y., Li, W., Wang, T.S., Qin, S.F., 2019. Thermochemical sulphate reduction of Sinian and Cambrian natural gases in the Gaoshiti-Moxi area, Sichuan Basin, and its enlightment for gas sources. Acta Geol. 93, 1754–1766.

Song, Z.Z., Liu, G.D., Luo, B., Zeng, Q.C., Tian, X.W., Dai, X., Jiang, R., Wang, Y.L., Li, Q., 2020. Logging evaluation of solid bitumen in tight carbonate in deep-buried and ultra-deep-buried strata of the central Sichuan Basin. Acta Sedimentol. Sin. 39, 197–211.

Sun, H.R., Huang, Z.L., Zhou, J.X., Leng, C.B., Gan, T., 2014. Rare earth elements geochemistry of fluorite in hydrothermal deposits and its geological significance. Journal of Petroleum and Mineralogy 33, 185–193.

Tissot, B.P., Welte, D.H., 1984. Petroleum Formation and Occurrence. Springer-Verlag, Berlin.

Tribovillard, N., Algeo, T.J., Lyons, T., Riboulleau, A., 2006. Trace metals as paleoredox and paleoproductivity proxies-An update. Chem. Geol. 232, 12–32.

Wang, T.G., Han, K.Y., 2011. On the primary oil and gas resources of the Meso-Neoproterozoic. Acta Pet. Sin. 32, 1–7.

Wei, G.Q., Wang, D.L., Wang, X.B., 2014. Characteristics of noble gases in the large Gaoshiti-Moxi gas field in Sichuan Basin. Petrol. Explor. Dev. 41, 533–538.

Wei, G.Q., Wang, Z.H., Li, J., Yang, W., Xie, Z.Y., 2017. Characteristics of source rocks, resource potential and exploration direction of Sinian and Cambrian in Sichuan Basin. Natural Gas Geoscience 28, 1–13.

Wei, G.Q., Xie, Z.Y., Song, J.R., 2015a. Characteristics and Genesis of Sinian-Cambrian Natural Gas in the Central Sichuan Basin Paleo-Uplift, Sichuan Basin, vol. 42. Petroleum Exploration and Development, pp. 702–711.

Wei, G.Q., Yang, W., Xie, W.R., Xie, Z.Y., Zeng, F.Y., Mo, W.L., Shen, J.H., Jin, H., 2015b. Sinian-Cambrian gas field formation conditions, accumulation model and exploration direction in Sichuan Basin. Natural Gas Earth Science 26, 785–795.

Wu, W., Luo, B., Luo, W.J., 2016. Another discussion on the origin of Sinian natural gas in the central Sichuan paleo-uplift in the Sichuan Basin. Natural Gas Geoscience 27, 1447–1453.

Xie, Z.Y., Li, J., Yang, C.L., Tian, X.W., Zhang, L., Li, J., Li, Z.S., Guo, J.Y., Xie, W.R., Guo, Z.Q., Qi, X.N., Hao, A.S., 2021. Geochemical characteristics of Sinian-Cambrian natural gas in central Sichuan paleo-uplift and exploration potential of Taihe gas area. Nat. Gas. Ind. 41, 1–14.

Xu, H.L., Wei, G.Q., Jia, C.Z., 2012. Tectonic evolution of Leshan-Longnüsi paleo-uplift and its control on Sinian reservoir formation. Petrol. Explor. Dev. 39, 406–416.

Yang, Y.M., Wen, L., Luo, B., Wang, W.Z., Shan, S.J., 2016. Characteristics of sinian natural gas accumulation in leshan-longnüsi paleo-uplift, Sichuan Basin. Petrol. Explor. Dev. 43, 179–188.
Zhang, P.W., 2019. Origin of Hydrogen Sulfide in the Ediacaran and Cambrian in the Central Sichuan Basin. China University of Petroleum (Beijing), Doctor's thesis.
Zhang, P.W., Liu, G.D., Cai, C.F., Li, M.J., Chen, R.Q., Gao, P., Xu, C.L., Wan, W.C., Zhang, Y.Y., Jiang, M.Y., 2019. Alteration of solid bitumen by hydrothermal heating and thermochemical sulfate reduction in the Ediacaran and Cambrian dolomite reservoirs in the Central Sichuan Basin, SW China. Precambrian Res. 321, 277–302.
Zhang, S.C., Liang, D.G., Li, M.W., Xiao, Z.Y., He, Z.H., 2002. Comparison of molecular fossils and oil sources in the Tarim Basin. Chin. Sci. Bull. 47, 16–23.
Zhao, L.Z., Wang, Z.C., Yang, Y., Duan, S.F., Wei, G.Q., Luo, B., Wen, L., Ma, S.Y., Feng, Q.F., Liu, J.J., Sun, X.P., Xie, W.R., 2020. Important discovery in the second member of Dengying Formation in well pengtan 1 and its significance, Sichuan Basin. China Petroleum Exploration 25, 1–12.
Zheng, P., Shi, Y.H., Zou, C.Y., 2014. Natural gas source analysis of Dengying Formation and Longwangmiao Formation in gaoshiti-moxi area. Nat. Gas. Ind. 34, 50–54.
Zhu, G.Y., Jin, Q., Wang, R., 2003. Effective source rock identification method. J. Univ. Pet. (China) 27, 6–10+9.
Zhu, L.Q., Liu, G.D., Song, Z.Z., Zhao, W.Z., Tian, X.W., Dai, X., Wang, Y.L., Yang, D.L., Li, Q., Jiang, L., Li, C.H., Hu, L., 2021. The differences in natural gas from the Dengying Formation in different areas of the north slope of the central Sichuan Paleo-uplift and its controlling factors—Taking Pengtan-1 and Zhongjiang-2 wells as examples. Petrol. Sci. Bull. 6 (3), 344–355.
Zhu, G.Y., Zhang, S.C., Liang, Y.B., Dai, J.X., Li, J., 2005. Isotopic evidence of the TSR genesis of high H_2S natural gas in Feixianguan Formation in northeastern Sichuan. Science in China (Series D: Earth Sci. 35, 1037–1046.
Zhu, G.Y., Zhang, S.C., Liang, Y.B., Ma, Y.S., Dai, J.X., Li, J., Zhou, G.Y., 2006. The characteristics of natural gas in Sichuan Basin and its source, 13, 234–248.
Zhu, Y.M., Hao, F., Zou, H.Y., Cai, X.Y., Luo, Y., 2007. Jurassic oils in the central Sichuan basin, southwest China: unusual biomarker distribution and possible origin. Org. Geochem. 38, 1884–1896.
Zou, C.N., Yang, Z., Dai, J.X., 2015. The characteristics and significance of conventional and unconventional Sinian-Silurian gas systems in the Sichuan Basin, central China. Mar. Petrol. Geol. 64, 86–402.